Journal of Petroleum Science and Engineering 189 (2020) 106971

Contents lists available at ScienceDirect

Journal of Petroleum Science and Engineering

journal homepage: www.elsevier.com/locate/petrol

The effect of upstream inlet choking and surfactant addition on the performance of a novel parallel pipe oil–water separator

Håvard S. Skjefstad [a,*], Marcin Dudek [b], Gisle Øye [b], Milan Stanko [a]

[a] Department of Geoscience and Petroleum, Norwegian University of Science and Technology, Norway
[b] Ugelstad Laboratory, Department of Chemical Engineering, Norwegian University of Science and Technology, Norway

ARTICLE INFO

Keywords:
Oil-water separation
Droplet size distribution
Surfactant
Inlet choking
Separation efficiency

ABSTRACT

This paper reports the effect of inlet choking and addition of surfactant on the performance of a parallel pipe oil–water separator. These two issues can have a strong effect on oil–water separation in real hydrocarbon production systems.

Experiments were performed with Exxsol™ D60 and salt water. Three choke settings were tested for flow rates in the range 300–500 L/min, with three inlet water cuts and three water extraction rates. The test matrix was run with and without added surfactant. The oil–water distribution and behaviour within the separator is also studied. Droplet size measurements were performed at the separator inlet for droplet size distribution generation in the form of cumulative volume plots.

The study shows that inlet choking has an overall negative effect on separator performance, especially for water-continuous inlet regimes. The maximum decrease in performance due to choking was 14 *pp*, while it was 4 *pp* due to addition of surfactant.

1. Introduction

Produced water management is a topic of increasing importance in the oil and gas industry. Produced water accompanies oil to surface, and in mature fields, often surpasses produced oil in terms of quantity. This is for instance seen on the Norwegian Continental Shelf, where 181 million standard cubic metres of produced water was reported for 2016, amounting to more than two times the amount of produced oil (NOROG, 2017). Produced water is the largest waste stream in oil production and contains a combination of organic and inorganic compounds, which when discharged may contaminate surface and underground water as well as soil (Zolfaghari et al., 2016). In order to secure safe disposal of produced water, the water must be separated from the oil and treated. Developing more efficient oil–water separator technologies and separation processes are important steps for securing safe disposal of produced water.

Although initially present as two separated phases, the turbulence, mixing and agitation through constrictions, choke valves and pumps will lead to oil–water dispersions (emulsions) being formed during production (Wong et al., 2015). These dispersions have to be separated during treatment processes before the fluids are exported (oil) or discharged/re-injected (water). In typical offshore topside processing, the fluids from an oil well are first separated in a gravity separator, where the gas, oil and water are segregated into individual streams based on their respective densities. Separated oil is pumped further to a secondary separator, often equipped with electrocoalescers to aid the growth of water droplets and speed up their sedimentation. At the same time, the produced water is treated in hydrocyclones (enhanced gravitational separation) or gas flotation units, where the removal of dispersed oil droplets is supported by their attachment to gas bubbles. Even though the bulk gravity separator alone often is insufficient to reach the desired quality of crude oil and water (Backi et al., 2018), its performance plays a key role in the efficiency of the further treatment process. In general, high water content in the crude oil and/or oil content in the produced water downstream the bulk separator can lead to the need for increased residence times and/or circulating flow back to the bulk separator inlet. Consequently, the performance of the first-stage separator will determine the production capacity and for that reason be crucial for the entire petroleum production chain (Fossen et al., 2006).

For a topside installation, the process stream is choked before entering the first stage bulk separator. This choking process serves as a large energy input to the stream, which causes subsequent dispersed-phase breakup into small droplets (emulsions). Emulsions are kinetically-stabilized liquid–liquid dispersions that are challenging to separate. What dictates the size of these droplets is the chemical composition and interfacial properties of the respective fluid components, and the

* Corresponding author.
E-mail address: havard.s.skjefstad@ntnu.no (H.S. Skjefstad).

https://doi.org/10.1016/j.petrol.2020.106971
Received 22 May 2019; Received in revised form 23 October 2019; Accepted 18 January 2020
Available online 22 January 2020

level of energy input in the droplet formation process. In complex fluid systems, such as crude oil, the kinetics of coalescence between droplets is thus an important factor to the separation process. Merging of micron-sized droplets can greatly speed up creaming or sedimentation of droplets (Andresen et al., 2000), as dictated by Stokes law of gravity separation, stating that the rising velocity is proportional to the square of the droplet radius. Coalescence, however, can also be hindered by the presence of crude oil-indigenous surface-active components (e.g. asphaltenes, resins or naphthenic acids), which can adsorb at the oil–water interface and stabilize the droplets against merging (Dudek et al., 2018). A second effect of topside transportation is lowering of pressure. For production streams containing dissolved CO_2, a reduction in pressure will result in an increase in pH. A pH increase will lead to higher surface charges on dispersed oil droplets, which further increases stability of the oil in water emulsions, hindering separation.

Knowledge of droplet size distributions and kinetics in oil–water dispersions/emulsions are thus important for sizing of separator equipment. Break up of two-phase oil–water flow and subsequent droplet distribution analysis has been reported in several publications in the past. In Schümann et al. (2015), Schümann et al. compared focus beam reflectance measurements (FBRM) and particle video microscopy (PVM) for droplet size measurement in oil–water dispersions. PVM measurements of known particle samples were shown to give correct droplet size distributions. Further, in Fossen and Schümann (2017), Fossen and Schümann investigated two-phase oil–water breakup over a butterfly valve at different pressure losses, water cuts and flow rates. However, the resulting effect on separator performance is rarely reported.

Separating oil and water on the seabed can mitigate some of the discussed issues of topside processing. By separating closer to the wells, and maintaining a high pressure, less problems with emulsion formation and emulsion stability is expected (Bringedal et al., 1999). In addition, separating close to the well means less mixing and turbulence, and the energy losses associated with transporting the water to surface are reduced. However, inlet choking (e.g wellhead choking) and stabilizing surfactants might still affect separator performance. The direct effect inlet choking and stabilizing surfactants has on separator performance is scarcely reported in the literature. Fossen et al. (2006) performed oil–water emulsion characterization in a vertical separator arrangement. Test fluids used were Exxsol^{TM} D60 and water with 3.5 wt% NaCl. Small amounts of crude oil (500 and 5000 ppm) and 20–30 vol% technical grade toluene was added to the Exxsol in order to increase stability of formed emulsions. Test fluids were mixed in an upstream T-section before passing through a needle valve for dispersion generation. The pressure loss over the needle valve was measured and reported. It was observed that the amount of emulsion formed increased with increasing pressure loss over the inlet needle valve. This led to a longer residence time requirement in the downstream separator to allow separation of the phases. Droplet sizes in formed emulsions were also measured, and it was seen that higher pressure loss over the inlet choke led to smaller droplets, again causing slower separation.

The aim of this paper is to investigate the direct effect inlet choking and stabilizing surfactant has on downstream bulk separator performance. Steady state measurements will be used to evaluate separator performance at varying inlet choke settings, water cuts and total flow rates. Pictures off occurring flow phenomena in the separator as well as droplet size distributions upstream the separator inlet will be used for supplementary evaluation. Droplet size distributions will be presented as cumulative volume fraction plots and Sauter mean diameters. The oil–water separation process is a balance between surface area effects (stabilization) and volume effects (speed of separation) and the Sauter mean diameter is an area weighted mean diameter often used to characterize oil–water dispersions (Angeli and Hewitt, 2000). The results of this paper will give a better understanding of how up-stream disturbances affect oil–water bulk separator performance. Subsequently, the paper results can give an indication of the potential benefit of subsea separation, where upstream disturbances are reduced.

2. Methodology

2.1. Separator concept

Experiments are carried out on a parallel pipe bulk oil–water separator concept prototype. The separator design was based on a state of the art subsea separator technology review (Skjefstad and Stanko, 2017), and is presented in Skjefstad and Stanko (2018) and Skjefstad and Stanko (2019). The concept has been named Multiple Parallel Pipe Separator (MPPS), and an illustration of the constructed prototype is given in Fig. 1. A multiphase oil–water feed stream enters at the separator inlet ($\dot{Q}_{in}$). The inlet has a tangential configuration, promoting initial cyclonic separation. The fluids pass through a set of novel phase rearranging internals, enforcing a radial to horizontal phase arrangement transition, before near complete separation is achieved in the horizontal pipe sections. Extraction of water ($\dot{Q}_{e_w}$) is performed in an upwards inclined pipe segment. The upwards inclination increases the water hold up at the extraction point, easing controlled extraction. Oil is extracted in its separate outlet ($\dot{Q}_{e_o}$). The prototype is constructed in 150.6 mm internal diameter (ID) transparent polyvinyl chloride (PVC) pipes, and has a total horizontal length of 6.1 m. Full dimensions of the prototype are given later in Fig. 3. Detailed information on design justifications can be found in Skjefstad and Stanko (2018), while a detailed overview of the inlet design and internal functionality and placement is found in Skjefstad and Stanko (2019).

2.2. Test facility

The test facility is a two-phase oil–water flow loop. Test fluids are distilled water with added 3.2 wt% NaCl and Exxsol^{TM} D60 with 0.015 g/L Oil Red O for phase distinction. Additionally, 750 ppm IKM CC-80 has been added to the water for bacterial growth inhibition, and 15 ppm of the surfactant Span®85 was added to the Exxsol^{TM} D60 for selected experimental points. Details on test fluid properties and behaviour is found in Section 2.4. A pipe and instrumentation diagram (P&ID) of the facility is given in Fig. 2.

The storage tank is a 6 m^3 (1.2 m diameter, 5.5 m long) gravity vessel providing baseline separation. Downstream the storage tank, a pump manifold boosts the respective clean phases to desired flow rate and water cut (WC). The pumps used in these experiments are centrifugal pumps, with respective flow capacities of 100–700 L/min (55 m max head). The pumps are controlled by 0–50 Hz frequency converters, 50 Hz constituting a maximum rpm of 2900. The flow rate and phase purities (densities) are monitored by two installed Coriolis flow meters (FT.1/2 and DT.1/2). The feed streams then enter a Y-junction, where they merge to a multiphase flow line. The multiphase flow line is a 13 m long 67.8 mm ID transparent PVC pipeline, leading to the inlet of the constructed separator prototype. A full-bore ball valve (VT.1) is installed 2 m upstream the separator inlet. This valve is used for choking of the inlet flow. The pressure loss over the valve is monitored by a differential pressure sensor (dPT.1), measuring from directly upstream to 5 ID downstream the valve. 1 m downstream VT.1 a particle video microscopy (PVM) probe insertion point for droplet size distribution measurements is placed. Pressure (PT.1) and temperature (TT.1) are measured at the prototype inlet. Two return lines are connected to the prototype outlets ($\dot{Q}_{e_w}$, $\dot{Q}_{e_o}$). The water return line is fitted with a third Coriolis flow metre (FT.3/DT.3), allowing monitoring of extraction rate (ER) and the purity of the extracted water. Both return lines are 67.8 mm ID PVC pipes leading back to the storage tank. Pressure is measured in both lines (PT.2/3), and both lines have choke valves installed for extraction rate adjustment. The water return line is fitted with an electrically controlled ball valve (VT.2), while the oil return line has a pneumatic membrane valve (VT.3). The span of installed sensors, as well as associated systematic error components are included later in Table 2. The reported systematic error components include linearity, hysteresis, quantization and data acquisition error.

Fig. 1. MPPS prototype.

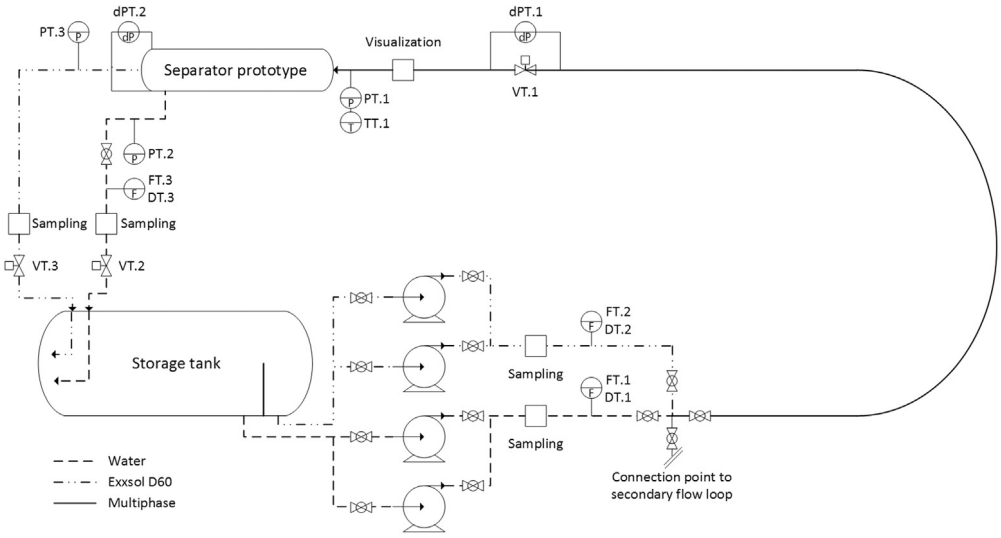

Fig. 2. Test facility P&ID.

The values reported are calculated with maximum span value and will hence represent a maximum. For errors reported later in Section 3, actual sensor readings have been used for error calculation, and the random error component associated with the respective readings has also been included.

2.3. Test parameters and procedure

All experiments carried out in this paper are steady state tests. The test matrix is given in Table 1. Three inlet choke levels were tested. The first was open valve (the valve is a fullbore valve, hence no induced pressure loss over VT.1), then $dPT.1 = 50$ mbar and $dPT.1 = 100$ mbar. Three total inlet flow rates ($\dot{Q}_{tot}$) were tested for each choke configuration, three inlet water cuts (WC_{in}) were tested for each flow rate, and three extraction rates were tested for each WC_{in}. The matrix was first completed with no added surfactant, then re-run with 15 ppm of the surfactant Span®85 added to the Exxsol™ D60. The total number of test points add up to 162.

Tests for one inlet choke configuration were carried out over one day. The system was then given one day resting before the next choke setting was tested. This was done to ensure complete phase separation in the storage tank in between testing, hence securing comparable initial conditions for the respective test configurations. The open valve tests were run first, followed by the 50 mbar then 100 mbar choke tests. The initial test point was $\dot{Q}_{tot} = 300$ L/min, 30% WC, 50% ER. The matrix was systematically executed by increasing ER, then WC, then total flow rate, until the final test point of $\dot{Q}_{tot} = 500$ L/min, 70% WC, 90% ER was reached.

All recorded parameters are listed in Table 2. Logging was performed at 5 Hz, with a log time of 60 s, giving a total of 300 samples per test point.

Table 1
Test matrix.

$dPT.1$ [mbar]	$\dot{Q}_{tot}$ [L/min]	WC_{in} [%]	ER [%]
–	300	30/50/70	50 70 90
	400	30/50/70	50 70 90
	500	30/50/70	50 70 90
50	300	30/50/70	50 70 90
	400	30/50/70	50 70 90
	500	30/50/70	50 70 90
100	300	30/50/70	50 70 90
	400	30/50/70	50 70 90
	500	30/50/70	50 70 90

Table 2
Recorded parameters including span and systematic error.

Tag	Parameter	Unit	Span	Error
FT.1	$\dot{Q}_1$	L/min	0–1000	±1.6e+00
FT.2	$\dot{Q}_2$	L/min	0–1000	±1.6e+00
FT.3	$\dot{Q}_3$	L/min	0–1000	±1.6e+00
DT.1	ρ_1	kg/m^3	750–1050	±5.7e−01
DT.2	ρ_2	kg/m^3	750–1050	±5.7e−01
DT.3	ρ_3	kg/m^3	750–1050	±5.7e−01
PT.1	P_1	barg	0–6	±5.8e−03
PT.2	P_2	barg	0–6	±5.8e−03
PT.3	P_3	barg	0–6	±5.8e−03
dPT.1	dP_1	mbar	0–2000	±1.9e+00
TT.1	T_1	°C	−30–122	±3.2e−01

Mean values of recorded parameters are used for subsequent calculation. The three Coriolis meters were used to adjust the inlet flow rate and water cut, monitor phase purities, determine the amount of water

extracted from the MPPS prototype, and the purity of the extracted water. The WC in the respective flow lines is determined by:

$$WC_i = \frac{\rho_i - \rho_o}{\rho_w - \rho_o} \quad (1)$$

Here, ρ_i is the measured density at DT.1/2/3, while ρ_w and ρ_o are the pre-determined temperature corrected densities of the water and Exxsol™ D60. For pure feed streams, WC_1 should be equal to 100% while WC_2 should be equal to 0%. From calculated WC and measured flow rates, the actual WC at the MPPS prototype inlet (WC_{in}) is calculated.

$$WC_{in} = \frac{WC_1\dot{Q}_1 + WC_2\dot{Q}_2}{\dot{Q}_1 + \dot{Q}_2} \quad (2)$$

$\dot{Q}_1$ and $\dot{Q}_2$ are the respective water and Exxsol™ D60 feed streams. When running experiments, $\dot{Q}_1$ and $\dot{Q}_2$ are adjusted such that the desired total flow ($\dot{Q}_{tot}$) and WC_{in} is reached. $\dot{Q}_{tot}$ is simply the sum of $\dot{Q}_1$ and $\dot{Q}_2$.

The amount of water extracted from the MPPS prototype is determined by the ER. The ER is the flow rate through the water extraction line (FT.3) divided by the flow rate in the water feed line (FT.1):

$$ER = \frac{\dot{Q}_3}{\dot{Q}_1} \quad (3)$$

As the test loop is a closed system, the water and Exxsol™ D60 phases will be contaminated over time. Microscopic droplets of water will be dispersed in the oil and vise versa. In order to give a performance measurement that is independent of occurring contamination, a WC ratio (WC_r) is calculated. The WC ratio is equal to the WC at the water extraction line (WC_3) divided by the WC at the water feed line (WC_1).

$$WC_r = \frac{WC_3}{WC_1} \quad (4)$$

A WC_r equal to 100% means that the extracted water from the MPPS prototype is of equal quality to the water leaving the baseline separator (storage tank). The separator performance reported in this paper (WC_r) is thus calculated as the purity of water extracted from the MPPS prototype (WC_3) divided by the purity of the feed water from the storage tank (WC_1). The accuracy of the stream water cut calculations are given by reported accuracy of installed Coriolis meters. For water cuts WC_1, WC_2 and WC_3, resulting errors are in the range ±0.25 pp, which is found through error propagation. For reported WC_r calculations in Section 3, the errors are in the range $\pm 0.35pp$.

Particle video microscopy (PVM) was used for droplet size measurement in this study. The probe utilized was a PVM V819 probe from Mettler Toledo. The probe provides real time in situ digital grey scale images for droplet size measurement. The technology uses a high resolution CCD camera and internal illumination to obtain high quality images. A reflector cap was fitted to the end of the probe for better image quality. The selected reflector cap has a 4 mm spacing from the probe window. The field of view is 1075 × 825 μm, with a resolution of 2 μm. The output image from the PVM has a resolution of 1360 × 1024 pixels, giving a conversion factor of 0.8 μm/pixel.

PVM pictures were taken for all flow rates and water cuts, at the 50% ER point. The PVM probe was inserted in the previously mentioned PVM insertion point, at a 45° angle. Pictures were taken at two heights, 0.15 and 0.85 ID from the top of the internal feed pipe wall. This gives a total of 18 picture series per inlet choke setting, and a grand total of 108 picture series. For every picture series, 100 pictures were taken at a frequency of 2 Hz. For future references, the 0.15 ID insertion point will be referenced as the top location, and the 0.85 ID point as the bottom location. These heights were chosen based on observed flow regimes at the separator inlet with open inlet choke, securing probe placement in the established water and oil layers for the 30% and 70% inlet WC test points respectively.

Table 3
Fluid properties @ 15 °C.

Fluid sample	ρ [kg/m^3]	μ [cP]	σ_{ow} [mN/m]
Water[b]	1021.05	1.20	16.1
Exxsol™ D60[b]	795.74	1.61	
Water[a]	1021.06	1.19	15.8
Exxsol™ D60[a]	795.76	1.61	
Water[bc]	1021.06	1.19	16.1
Exxsol™ D60[bc]	795.78	1.60	
Water[ac]	1021.04	1.21	16.2
Exxsol™ D60[ac]	795.75	1.59	

[a]After experiment.
[b]Before experiment.
[c]With 15 ppm Span®85.

Photos of flow phenomena in the horizontal pipe sections were taken to improve the understanding of measured performance trends. Pictures were taken at the start and end of the respective pipe sections, as illustrated in Fig. 3. The figure also includes overall dimensions of the MPPS prototype, as well as the distance between the picture points.

Additionally, pictures were taken directly upstream the MPPS inlet (in the 67.8 mm ID feed-pipe) for inlet flow regime determination.

The following test procedure was followed for all test points:

1. Total flow, WC_{in} and ER adjusted to desired values
2. Inlet choke valve adjusted for desired dPT.1 value
3. System operated for five times the corresponding MPPS residence time for steady state behaviour. Respective residence times vary from approximately 30 to 50 s
4. When ER equal to 50%, PVM inserted at respective heights and 100 pictures taken
5. PVM removed
6. If PVM pictures taken, subsequent steady state operation period of five times the corresponding MPPS prototype residence time
7. Picture taken of the inlet flow regime
8. Separator performance logged
9. Pictures taken of flow distribution at entrance and exit of horizontal pipe segments

2.4. Fluid characterization

In order to validate comparability of results, fluid samples from the storage tank were collected before and after each test campaign for density, dynamic viscosity and interfacial tension (IFT) determination. Density measurements were performed with an Anton Paar DMA™ 5000M densitometer. Viscosities were measured with an Anton Paar Physica MCR 301 rheometer. Densities and viscosities were measured between 10–20°C with 2.5°C intervals. The mean values at 15°C are reported in Table 3. The IFT between the respective oil and water samples were measured with a DataPhysics SVT20 spinning drop video tensiometer at 15°C, and is also reported in Table 3. Each measurement was repeated twice. The standard deviation for the viscosity tests is in the range of 1%, while it is between 1 and 4% for the IFT measurements.

The measured reference density curves for water and Exxsol™ D60 used in reported experiments are given in Eqs. (5) and (6).

$$\rho_w = -0.0048T_1{}^2 - 0.0722T_1 + 1023.2 \quad (5)$$

$$\rho_o = -0.7319T_1 + 806.72 \quad (6)$$

A series of IFT measurements were performed to characterize the interfacial properties of the studied system. It was found that the used Exxsol™ D60 and water already exhibited interfacial activity, even before adding surfactant. By performing tests in which one of

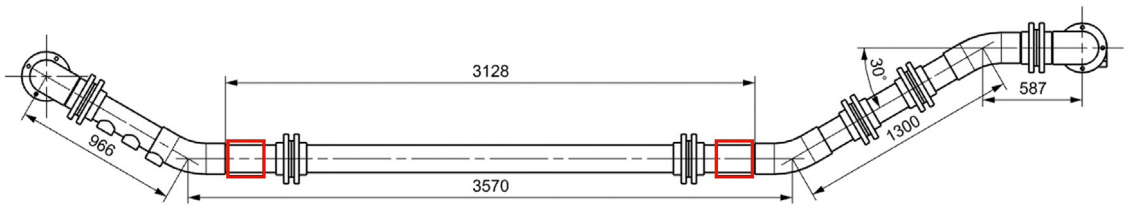

Fig. 3. Prototype dimensions [mm] with illustrated picture location.

the phases was replaced with a clean sample of Exxsol^{TM} D60 or salt water (e.g. freshly prepared salt water with the Exxsol^{TM} D60 sampled from the test facility storage tank), it was observed that the IFT did not differ from the values obtained from the sampled Exxsol^{TM} D60 and water. All measurements were approximately 16 mN/m, which is remarkably close to other crude oil and brine systems reported in literature (Tichelkamp et al., 2015; Dudek et al., 2017). By contrast, the IFT for a pure (non-sampled) salt water and Exxsol^{TM} D60 system was close to 40 mN/m. Measurements were also performed on a system without the biocide — pure salt water and pure Exxsol^{TM} D60 with the addition of the Oil Red O dye. These revealed higher IFT values (approximately 25 mN/m), and also considerably slower equilibration, compared to the systems with the biocide present. Therefore, it is suspected that the biocide added to the system, which appears to some extent be both oil- and water-soluble, is mostly responsible for the interfacial activity demonstrated in this system.

Additional IFT measurements and bottle tests were performed on the fluids before adding the surfactant to pre-determine its effect and avoid under- or overdosage. IFT measurements were done with the above-mentioned spinning drop tensiometer. The bottle tests were conducted by adding appropriate amounts of oil (with and without the surfactant) and water to a vial (with similar proportions as in the experimental matrix), mixing them at 10 000 rpm for 30 s and visually following the separation. All of these tests were performed in room temperature (approximately 23 °C).

The IFT measurements with surfactant revealed that adding 10 ppm of surfactant to the Exxsol^{TM} D60 had virtually no effect on the IFT of oil and water, whereas the addition of 25 ppm of Span®85 to the sampled oil phase caused the IFT to be lowered to 13.5 mN/m, and 50 ppm of the surfactant resulted in the IFT value of approximately 12 mN/m. Conducted bottle tests reflected these results. In the bottle tests, 10 ppm of surfactant did not significantly change the emulsion behaviour, compared to the system without the additive. After adding 25 ppm of the surfactant, the formation of a stable emulsion phase at 30% and 50% WC could be observed, which prolonged the separation process several times. This effect was multiplied when the higher concentration of surfactant (50 ppm) was tested, where the separation took more than one hour. In both cases, however, the separation was quite quick at the highest water cut. Based on the observed bottle test results and previous experience that over-dosage of surfactant can lead to extremely stable emulsions, it was decided that 15 ppm of the surfactant was a fitting concentration for the large scale separator tests.

2.5. Droplet size measurement

Recorded PVM pictures were used for calculating droplet size distributions. For each test point, all captured pictures were analysed with an image analysis software (SOPAT GmbH, Germany), automatically registering individual droplet diameters. Subsequently, recorded droplet diameters were used to generate cumulative volume fraction (Q_f) distributions (Eq. (7)) for the respective test points. In Eq. (7), d_i is the individual recorded droplet diameters in the respective samples. Plots are given for d ranging from 1 to 600 μm, 600 μm being above d_{max} for all test points.

$$Q_f(d) = \frac{\sum \pi {d_i}^3/6 \quad for \quad d_i \le d}{\sum \pi {d_i}^3/6 \quad for \quad d_i \le d_{max}} \tag{7}$$

Table 4
Flow regime at MPPS inlet.

$\dot{Q}_{tot}$ [L/min]	WC_{in} [%]	No choke	50 mbar choke	100 mbar choke
300	30	SM	Dw/o	Dw/o
	50	SM	Do/w	Do/w
	70	SM	Do/w	Do/w
400	30	SM	Dw/o	Dw/o
	50	SM	Do/w	Do/w
	70	SM	Do/w	Do/w
500	30	Do/w + Dw/o	Dw/o	Dw/o
	50	Do/w+Dw/o	Do/w	Do/w
	70	Do/w+Dw/o	Do/w	Do/w

The SOPAT image analysis software is thoroughly outlined in Panckow et al. (2017), and has seen recent applications in Riegler et al. (2019) and Bliatsiou et al. (2018). In addition to cumulative volume fraction plots, the Sauter mean diameter (d_{32}) and the 50% median volume based diameter (d_{v50}) are provided for additional trend analysis.

Determining the accuracy of performed counting is challenging, as different counting approaches will give varying results. A manual counting procedure was considered for this study, however, small droplets were difficult to determine, and consistency in the counting was deemed unsatisfactory with a manual approach. An automatic counting procedure was therefore chosen, as an increased consistency gives a better ground for comparison of respective test points. As the accuracy of presented droplet sizes are not defined, results are solely used as supplementary information to established separator performance in an effort to provide additional grounds for trend analysis. A picture of a completed droplet registering has been included in the appendix, Fig. A.17, which gives an understanding of the underlying accuracy.

3. Results

3.1. Inlet flow regime

The flow regime at the inlet was mapped for all test points. Identification was based on illustrations given by Trallero et al. (1997), and previous identification by the authors Skjefstad and Stanko (2019). Four different flow regimes were identified: stratified mixed (SM), dispersed oil in water and dispersed water in oil (Do/w+Dw/o), dispersed oil in water (Do/w) and dispersed water in oil (Dw/o). Regimes for the respective test points are listed in Table 4.

Recorded flow regimes were similar for the no-surfactant and surfactant tests. Pictures of captured flow regimes are included in Appendix.

3.2. Separator performance and flow phenomena

The calculated WC_r for the no-surfactant test points are given in Fig. 4. The calculated WC_3 for the same test points are included in Appendix, Fig. A.18. In Appendix, the reader will also find tables of all recorded data, with associated errors, for the respective test points. The maximum error in reported WC_r values is 0.4 pp. Included errors are linearity, hysteresis, quantization, data acquisition and random error in the measurements.

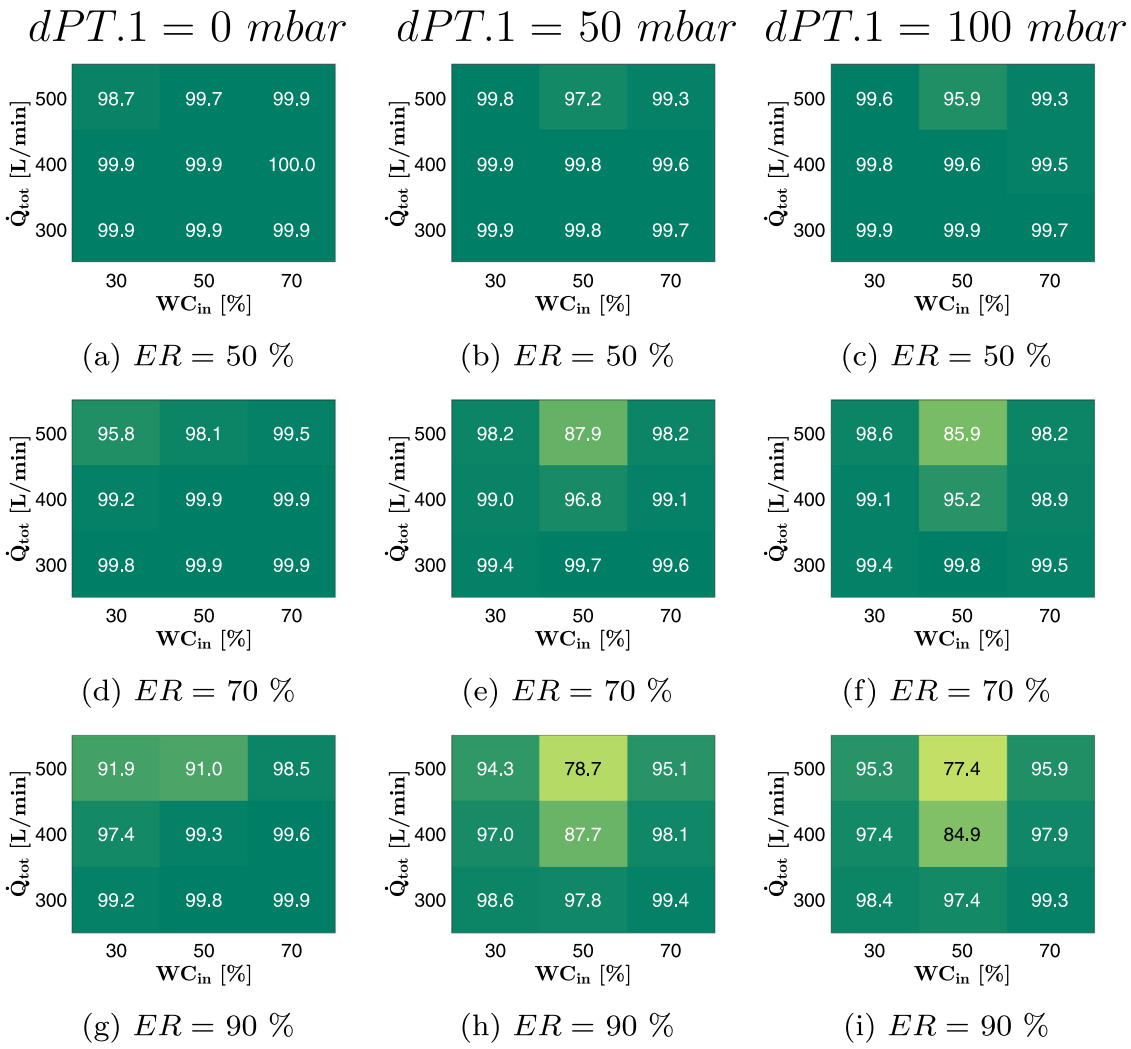

Fig. 4. WC_r [%] results for $dPT.1 = 0$, 50, 100 mbar and $ER = 50$, 70, 90% for the no surfactant tests.

The effect of inlet choking is clearly visible when looking from Fig. 4(a), 4(d), 4(g) (No choke), to Fig. 4(b), 4(e), 4(h) (50 mbar choke) and Fig. 4(c), 4(f), 4(i) (100 mbar choke). At 50% ER, a slight decrease in performance is observed when applying inlet choking for an inlet WC of 50% and a total flow rate of 500 L/min. For the same flow rate, a slight increase in performance is seen for 30% WC_{in} when moving from no-choke to applied inlet choking. The same trend is observed when increasing the extraction rates. The reduction in performance is more severe for high total flow rates, high pressure drops over the choke, and medium inlet water cut. The maximum reduction observed in WC_r is 14 pp when compared against the no choking case. For low inlet water cut, the effect of inlet choking on WC_r is negligible or, for the high total flow rate case, improving separation with a maximum of 3 pp.

Captured flow phenomena in the horizontal pipe sections supports observed trends in logged performance. In Figs. 5 to 8, flow phenomena at the start and end of the horizontal pipe sections are given. Included pictures are for 30% and 50% inlet WC, with $\dot{Q}_{tot}$ = 400 and 500 L/min, displaying flow phenomena with open inlet choke and for a dPT.1 pressure of 100 mbar. Flow phenomena were similar in both pipe segments, and for this reason, pictures of only one pipe have been included. Observed trends for the 70% WC_{in} test points were the same as for the 50% WC_{in}, and are not shown.

Figs. 5 and 6 shows the flow distribution at 50% inlet water cut.

From presented pictures it is clearly seen how inlet choking affects dispersion at both the start and end of the horizontal pipe sections. A clear increase in dispersion layer thickness is observed at the end of the horizontal pipe, and an increase in flow rate is observed to further increase both the layer thickness and the effect of inlet choking. A result of this increased dispersion layer is an increased chance of extracting the dispersion with the water at high extraction rates. This corresponds well with reported data in Fig. 4, where a drastic decrease in WC_r at 90% ER is observed for 50% WC_{in} at $\dot{Q}_{tot}$ = 400 and 500 L/min, the latter being worse. It should also be noted that the forming dispersion layer in the pipes is water-continuous. A clear/sharp boundary is observed between the pure oil layer and dispersion layer, while the boundary between the water and dispersion layer is more gradual.

A different behaviour is observed for the 30% inlet WC test points (Figs. 7 and 8)

From presented pictures there is little to no observed effect of inlet choking. For $\dot{Q}_{tot}$ = 400 L/min, both entry and exit of the horizontal pipe section looks unchanged. At $\dot{Q}_{tot}$ = 500 L/min a slight decrease in the formed dispersion layer thickness is detectable for the 100 mbar inlet choke case. This is again consistent with presented data in Fig. 4. At 300 and 400 L/min, no significant effect of inlet choking is detected for the 30% WC_{in} test points. However, at 500 L/min, an increase in WC_r is observed at high ER. Again, the formed dispersion layer at the exit of the separator pipes is seen to be water-continuous.

The calculated WC_r for the 15 ppm Span®85 test points display the same trends as for the no-surfactant tests. A decline in WC_r is observed with increasing pressure drop over the inlet choke. However, an exception from the no-surfactant trend is observed for the 30% inlet

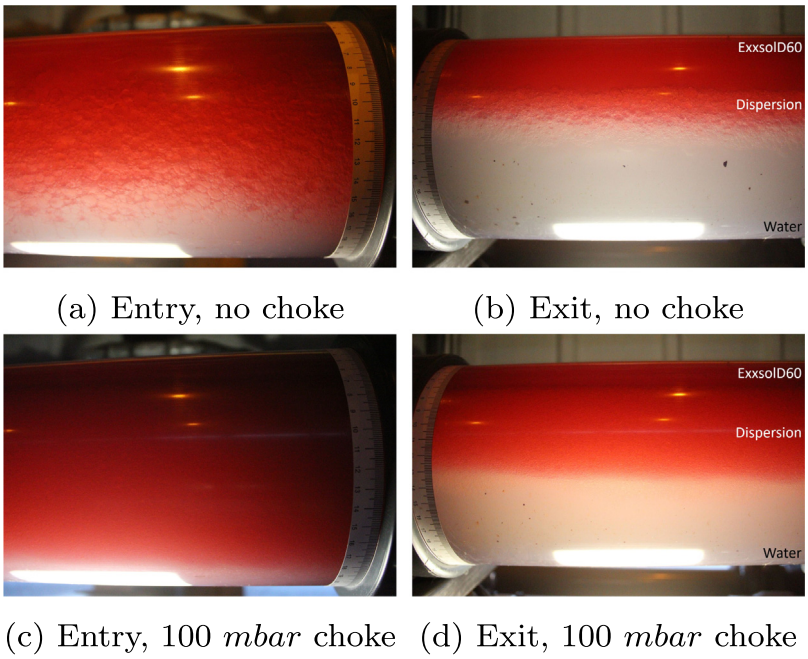

Fig. 5. Flow phenomena at the start and end of the horizontal pipe sections for the no-surfactant tests at $\dot{Q}_{tot}$ = 400 L/min, WC_{in} = 50 % and ER = 90%. Pictures are given for no choke and 100 mbar choke.

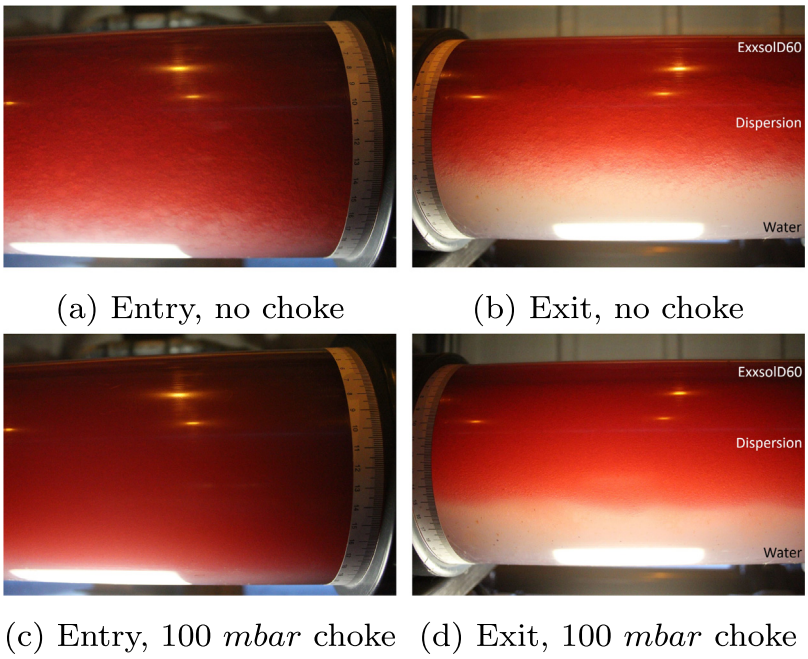

Fig. 6. Flow phenomena at the start and end of the horizontal pipe sections for the no-surfactant tests at $\dot{Q}_{tot}$ = 500 L/min, WC_{in} = 50 % and ER = 90%. Pictures are given for no choke and 100 mbar choke.

WC test points. For the system with no surfactant (Fig. 4), an increase in WC_r was observed at $\dot{Q}_{tot}$ = 500 L/min when the pressure loss over the inlet choke was increased. This is not the case after adding surfactant. For the surfactant case, the WC_r is stable when going from open choke to 50 mbar pressure loss, and drops when increasing the pressure loss to 100 mbar. Plots of WC_r and WC_3 for the surfactant tests are included in Appendix, Figs. A.19 and A.20. Again, the maximum error in reported WC_r values is 0.4 pp.

In Fig. 9 the effect of adding surfactant is illustrated. The figure shows calculated WC_r for the surfactant tests (Fig. A.19) subtracted the WC_r of the no-surfactant tests (Fig. 4). The results are given in percentage points (pp), where a negative value indicates a decrease in performance, and a positive value indicates an increase in performance.

Adding surfactant has a general negative effect on the separator performance for the 50% and 70% WC_{in} test points. A maximum decrease of 4 pp is observed for $\dot{Q}_{tot}$ = 500 L/min, at 50% WC_{in} and 70% ER. However, an increase in performance is observed for the 30% WC_{in}, $\dot{Q}_{tot}$ = 500 L/min test point at the no choke and 50 mbar choke settings.

In Figs. 10 and 11, captured flow phenomena for the surfactant tests are shown. The figure displays flow phenomena at the horizontal pipe exit for the same test points as in Figs. 5 to 8. Comparing these

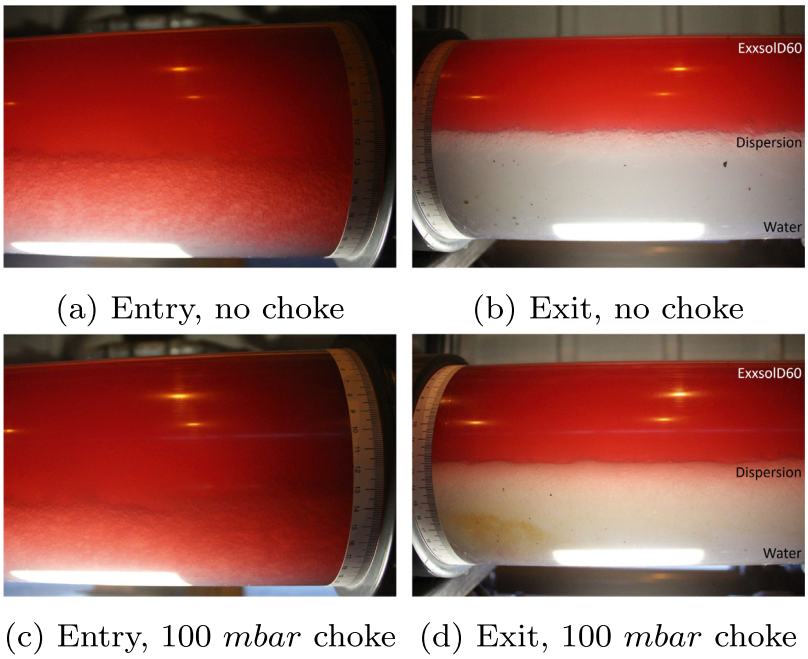

Fig. 7. Flow phenomena at the start and end of the horizontal pipe sections for the no-surfactant tests at $\dot{Q}_{tot}$ = 400 L/min, WC_{in} = 30 % and ER = 90%. Pictures are given for no choke and 100 mbar choke.

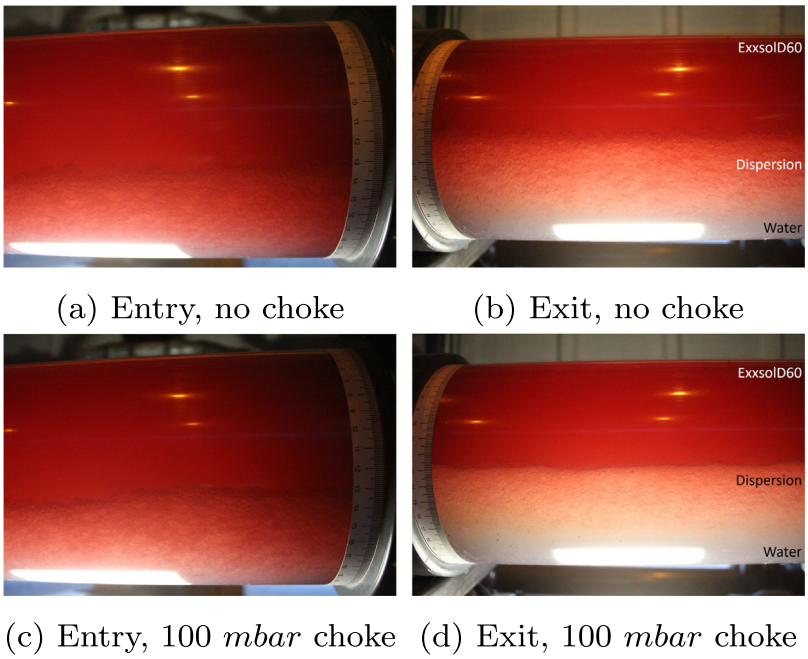

Fig. 8. Flow phenomena at the start and end of the horizontal pipe sections for the no-surfactant tests at $\dot{Q}_{tot}$ = 500 L/min, WC_{in} = 30 % and ER = 90%. Pictures are given for no choke and 100 mbar choke.

figures, there is no significant change detected from adding surfactant at a 50% inlet WC, except a small increase in the dispersion layer for the no choke test points. For the 30% WC_{in} test points however, a small change is noted. For the no choke test point at $\dot{Q}_{tot}$ = 500 L/min, the formed dispersion layer is observed to be more "compact" and smaller in size compared to the no-surfactant test in Fig. 8. At the same time, the 100 mbar choke test points display a larger dispersion layer compared to the equivalent no-surfactant test points. This does again support results reported in Fig. 9, where an increase in WC_r is seen for $\dot{Q}_{tot}$ = 500 L/min, 30% WC_{in} no-choke, while a drop in WC_r is seen for all flow rates at 30% WC_{in} at 100 mbar inlet choking. Similarly to the no-surfactant tests, formed dispersion layer in the separator pipes is seen to be water-continuous.

3.3. Droplet distributions

Droplet distributions are presented as cumulative volume fraction vs. droplet diameter plots. Markers are included at 50 μm intervals. The plot gives a representation of the accumulated volume of all droplets up to a specified diameter, divided by the total volume of all droplets recorded. When comparing plots of test points with the same inlet WC, a shift to the left will indicate more, and smaller droplets

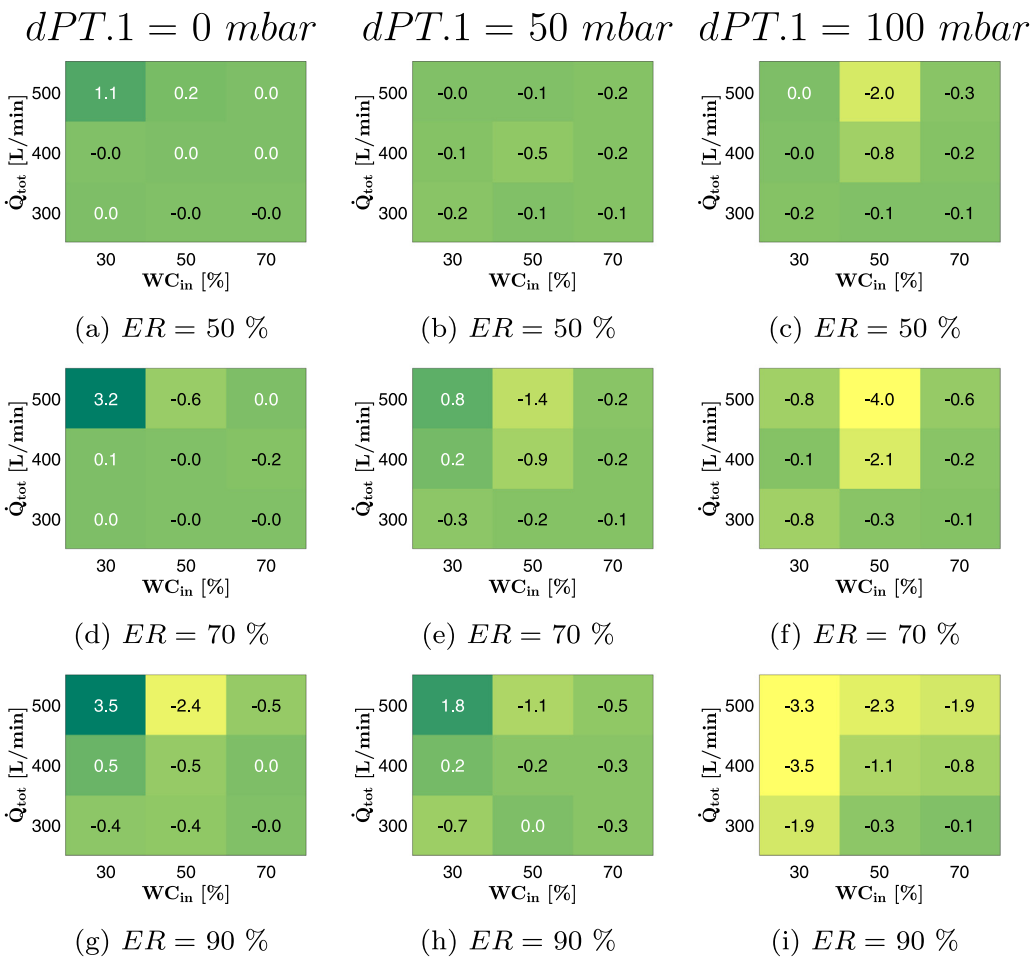

Fig. 9. Difference [*pp*] between the surfactant and no-surfactant WC_r results for $dPT.1 = 0$, 50, 100 mbar and $ER = 50$, 70, 90%.

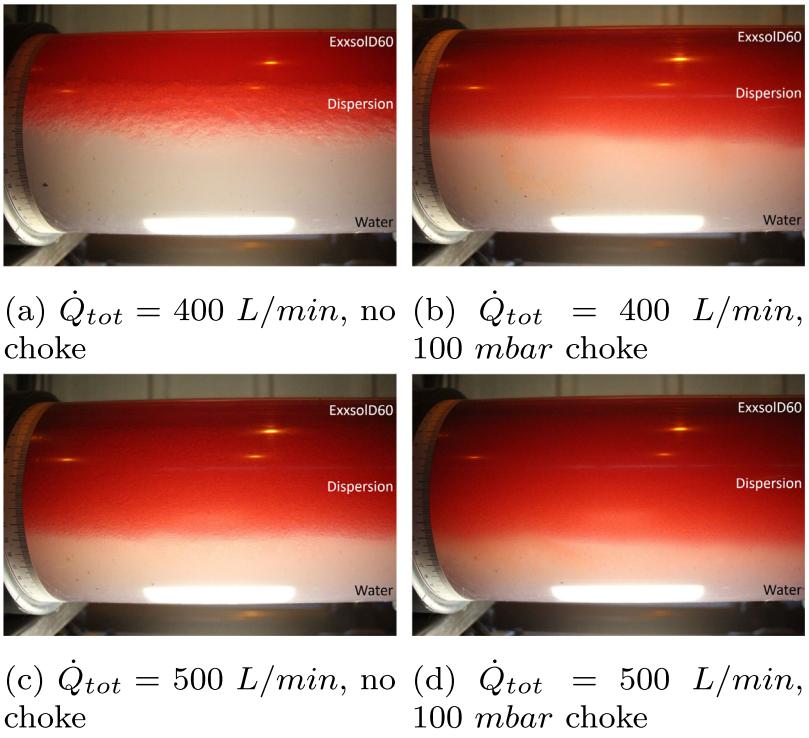

Fig. 10. Flow phenomena at the exit of the horizontal pipe sections for the 15 ppm Span®85 tests at $WC_{in} = 50$ % and ER = 90%. Pictures are given for no choke and 100 mbar choke.

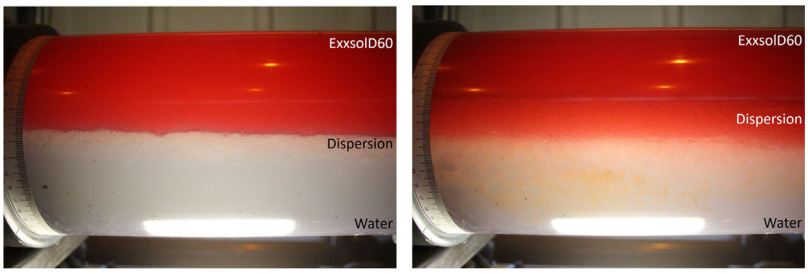

(a) $\dot{Q}_{tot} = 400\ L/min$, no choke (b) $\dot{Q}_{tot} = 400\ L/min$, 100 $mbar$ choke

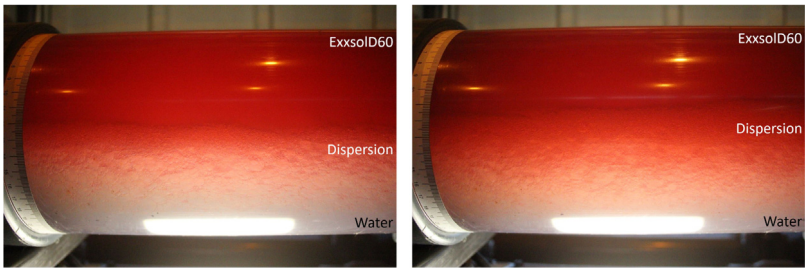

(c) $\dot{Q}_{tot} = 500\ L/min$, no choke (d) $\dot{Q}_{tot} = 500\ L/min$, 100 $mbar$ choke

Fig. 11. Flow phenomena at the exit of the horizontal pipe sections for the 15 ppm Span®85 tests at WC_{in} = 30 % and ER = 90%. Pictures are given for no choke and 100 mbar choke.

being recorded, while a shift to the right indicates fewer and larger droplets being recorded. Plots are however sensitive to large drops, as the volume is a function of the diameter cubed. This means that a rightward shift in the plotted graph can be induced by a few large droplet recordings, which does not necessarily represent the overall trend for the test point. In addition, plotted distributions only captures the fraction of phases that are dispersed. This means that for test points with inlet regimes that are not fully dispersed, a cumulative volume fraction of 1 will not represent the actual total volume fraction of the respective phase, which would be the sum of all droplets and the continuous part. An example is made for the no choke test points in Table 4, with a Do/w + Dw/o flow regime. This means that the bottom part of the inlet pipe has a continuous water layer with dispersed oil droplets, while the top part of the pipe has a continuous oil layer with dispersed water droplets. If droplet sizes are measured at the bottom of the pipe, oil droplets in water will be observed. A plotted cumulative volume fraction value of 1 will then represent the volumetric amount of the oil phase which is dispersed in the water. The actual volume fraction of oil is the sum of the dispersed oil and the continuous oil in the top part of the pipe.

Based on reported flow regimes at the separator inlet, bottom location data (oil drops in water) are presented for the 50% and 70% WC_{in} test points, while top location data (water droplets in oil) are presented for the 30% WC_{in} test points. The average number of droplets captured per test point (droplet diameters used for distribution calculation) was 2402 for the no-surfactant tests and 3457 for the surfactant tests. The overall minimum number of droplets captured for one test point was 874.

In Fig. 12, results for 50% WC_{in} at dPT.1 = 100 mbar and increasing flow rates are given. It is clear that an increase in flow rate results in a leftward shift in the distribution. This indicates an increased fraction of smaller droplets, and hence more difficult separation conditions. For $\dot{Q}_{tot}$ = 400 and 500 L/min, the addition of surfactant is observed to cause a further shift to the left.

The same trend as in Fig. 12 is observed for 50 mbar choke and the 70% WC_{in} test points, which distributions are included in Appendix.

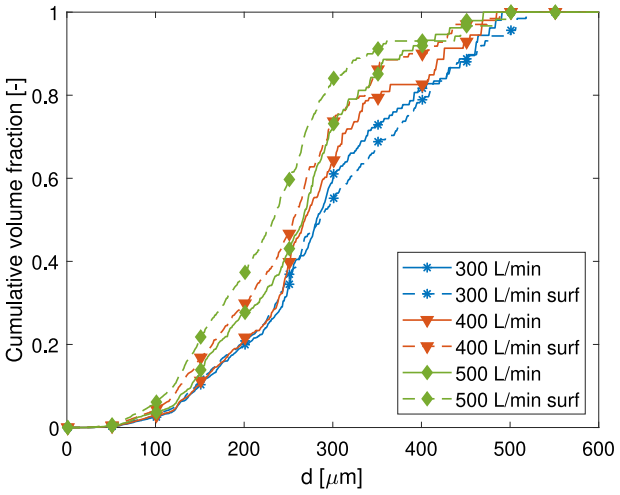

Fig. 12. Cumulative volume fraction for WC_{in} = 50 %, $dPT.1$ = 100 mbar.

The distribution for 30% WC_{in} at $dPT.1$ = 100 mbar is given in Fig. 13.

In the sub 250 μm droplet diameter range, the trend is similar to the 50% and 70% WC_{in} test points. Above 250 μm, however, the trends are not as consistent. In the case of two flow rates (300 and 500 L/min), the addition of surfactant results in a rightward shift of the cumulative fractions, indicating that larger droplets are detected. An opposite observation is made for the remaining flow rate, where the additive is seen to decrease the water droplet sizes. It should be noted that in this case, a significant contribution from the above 500 μm droplets is present, which can influence the outcome of the plot, as previously discussed.

A different trend is observed for the no choke test points. Fig. 14 displays the distribution for the 30% WC_{in} cases.

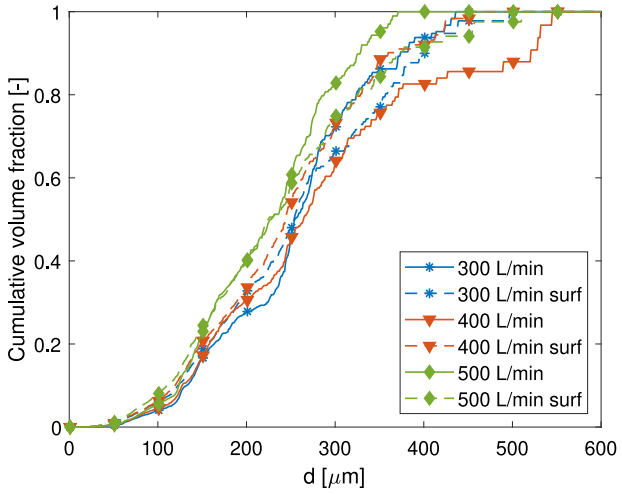

Fig. 13. Cumulative volume fraction for WC_{in} = 30 %, $dPT.1$ = 100 mbar.

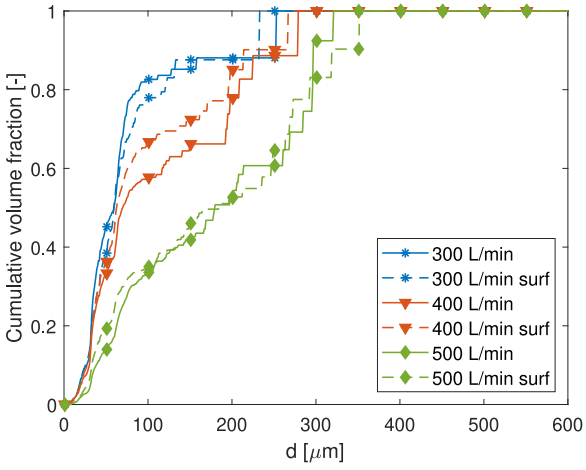

Fig. 14. Cumulative volume fraction for WC_{in} = 30 %, no choke.

The graph shows a shift to the right for increasing flow rates. Although higher flow rates usually mean higher turbulence levels, and hence smaller droplet sizes, it is in this case believed that the level of dispersion of both phases influence the results. For the no choke test points, the majority of the oil and water exists as continuous phases. At low flow rates, most of the dispersed droplets will be smaller droplets that were not separated out in the storage tank and thus recirculated in the test loop. At higher flow rates however, larger droplets will start to get entrained and dispersed in the respective continuous phases. This explanation is supported by flow regimes reported in Table 4, and in pictures given in Appendix. A similar trend is seen for the 50% and 70% WC_{in} test points. The recirculation of small droplets can be illustrated with simplified Stoke's law terminal creaming/sedimentation velocity estimations. Given reported fluid properties in Table 3, a tank diameter of 1.2 m (with 90% liquid area) and an effective separation length of 5 m, a 50 μm diameter droplet will achieve a creaming/sedimentation distance of 0.23 m and 0.18 m respectively, for a total flow rate of 300 L/min. This is not sufficient to fully separate in the storage tank.

In Fig. 15 the effect of inlet choking is shown. The figure shows cumulative volume plots for $\dot{Q}_{tot}$ = 500 L/min, 50% WC_{in} test points at the respective choke settings.

It is clear that the no-choke test points have the smallest droplets, which agrees with the previous explanation. Of the two choke settings (where the inlet regimes are fully dispersed), 50 mbar displays overall

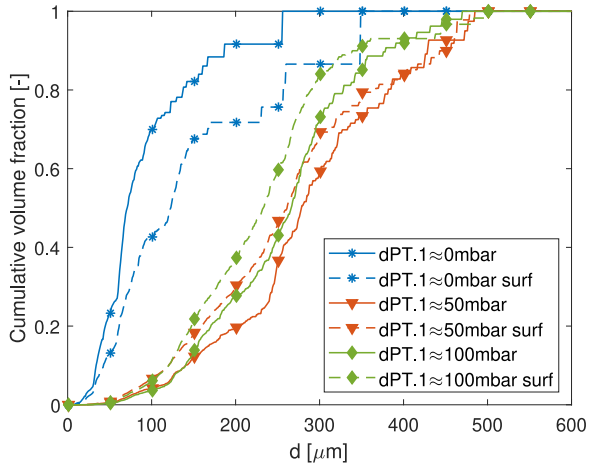

Fig. 15. Cumulative volume fraction at respective droplet diameters and choke settings for $\dot{Q}_{tot}$ = 500 L/min, WC_{in} = 50 %.

Table 5
Bottom location $d32$ [μm] data for **no surfactant** and *surfactant* test points.

WC_{in} [%]	$dPT.1$ [mbar]	Total flow rate [L/min]					
		300		400		500	
	–	**90.8**	*33.7*	**99.4**	*80.3*	**89.8**	*152.9*
30	50	**253.6**	*236.9*	**245.3**	*220.5*	**205.5**	*191.1*
	100	**212.4**	*212.9*	**203.1**	*207.5*	**185.2**	*186.2*
	–	**51.7**	*45.9*	**44.8**	*59.4*	**63.1**	*86.9*
50	50	**278.0**	*244.0*	**266.2**	*231.7*	**231.6**	*203.0*
	100	**243.3**	*241.3*	**234.0**	*207.8*	**216.9**	*188.6*
	–	**37.1**	*40.2*	**48.4**	*67.3*	**61.6**	*63.6*
70	50	**221.8**	*196.4*	**210.4**	*184.6*	**195.9**	*172.2*
	100	**207.2**	*197.1*	**191.7**	*168.8*	**161.0**	*154.3*

larger droplet sizes, which agrees with expectations (smaller droplets for larger energy input) and presented WC_r results. For the choked inlet streams, adding surfactant is seen to shift the distribution to the left, indicating smaller droplets and hence slower separation. This also agrees with reported WC_r data. The distribution trends are the same for the 70% WC_{in} test points.

The top and bottom cumulative volume fraction distributions for the $\dot{Q}_{tot}$ = 500 L/min, 30% WC_{in} test point are given in Fig. 16.

The top distribution displays a similar trend as for the 50% WC_{in} case, however, a slight shift to the right is observed when adding surfactant. A rightward shift for the open and 50 mbar choke settings is more clear for the bottom location distribution, which supports reported WC_r results for these test points.

The $d32$ data for all bottom location recordings are presented in Table 5.

For the water-continuous inlet regimes (50 and 70% inlet water cut) a clear trend is observed. Smallest droplets are seen for the no choke test points, which corresponds with distribution trends and previous explanations. For choked test points, droplet sizes are seen to decrease with increasing choke level, flow rate and inlet WC. Further, a reduction in d_{32} is observed for the choked test points when surfactant is added. For the case with open inlet choke, a slight increase in d_{32} is observed for 5 out of 6 points.

For the 30% WC_{in} test points, a slightly different trend is observed. For the choked test points, the trend is the same as for the water-continuous, with decreasing d_{32} for increased choke level, flow rate and the addition of surfactant. For the no choke test points, both an increase and reduction in d_{32} is observed for increasing flow rates and addition of surfactant. A general observation to all test points is that process parameters have an equal if not greater effect on droplet sizes compared to addition of surfactant.

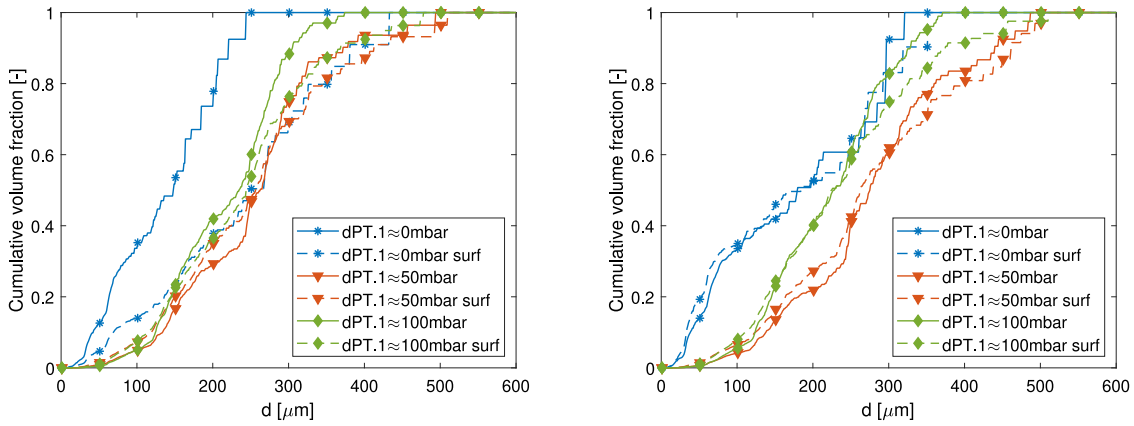

(a) bottom location (b) top location

Fig. 16. Cumulative volume fraction for $\dot{Q}_{tot}$ = 500 L/min, 30% WC_{in}.

The d_{v50} data display similar trends as reported for the d_{32} data, and is included in Appendix.

3.4. Discussion

From presented results it is clear that inlet choking has a negative effect on the separator performance for the water-continuous inlet regimes. For the oil-continuous inlet regimes, with no surfactant added, choking led to similar or slightly improved separator performance. The recorded dispersion layer present at the separator outlet was observed to be water-continuous. Results thus indicate the dispersion of oil droplets into the water phase as being the largest contributor to decreased separator performance when applying inlet choking.

For water-dominated inlet regimes, separator performance is seen to decrease for increasing total flow rates, extraction rates and level of inlet choking. Higher flow rates lead to higher turbulence levels, causing increased entrainment and breakage. Inlet choking serves as an energy input to the flow, which again leads to dispersion being formed. High extraction rates cause parts of the present dispersion layer at the separator outlet to be extracted with the water phase, decreasing performance. Moreover, addition of surfactant further reduced separator performance in this regime, which again can be explained by smaller and more stable oil droplets forming when surfactant is added. This is supported by the reported cumulative volume fraction plot in Fig. 12, corresponding well with the recorded performance data presented in Figs. 4 and 9. From Fig. 4, a decrease in WC_r is observed for increasing total flow rates at 50% WC_{in} and $dPT.1$ = 100 mbar. In Fig. 9, it is also seen that WC_r decreases for $\dot{Q}_{tot}$ = 400 and 500 L/min when adding surfactant, while no significant change is observed for $\dot{Q}_{tot}$ = 300 L/min. Reported d_{32} calculations further support these observations, decreasing with increased choking, flow rate and surfactant addition. For the no choke test points (with stratified flow at the inlet), an increase in d_{32} was observed when adding surfactant. A plausible explanation for this phenomenon is that addition of surfactant caused an increase in entrainment and dispersion. The droplets created in this process are larger than droplets recirculated in the flow loop (which are present in the respective continuous phases), hence causing an increase in d_{32}.

For the oil dominated inlet regimes, results indicate that inlet choking in certain cases can lead to better separation of water droplets dispersed in oil. The fact that only a water-continuous dispersion layer was observed at the separator outlet indicates that any oil-continuous dispersion present at the separator inlet was fully separated, and that performance for the 30% WC_{in} test points is dictated by the amount of water-continuous dispersion formed in the choking process, or downstream in the separator inlet. The fact that the dispersion created by the inlet choke is believed to be oil-continuous, thus limiting the amount of water-continuous dispersion being formed, can explain why no significant decrease in performance was observed when applying choking. This is also supported by the thin dispersion layers observed at the separator outlet for the 30% inlet WC test points. From reported WC_r results, an increase in separator performance was observed for the $\dot{Q}_{tot}$ = 500 L/min, 30% WC_{in} test points when adding surfactant for the no choke or moderate choke (50 mbar) configurations. This observation was supported by reported cumulative plots (Fig. 16). A possible explanation can be that the addition of surfactant causes an increase in the number of formed water droplets, which can lead to an increase in coalescence. This can again indicate that the added surfactant mostly increases oil droplet stability, and not water droplet stability. The drop in performance observed for the 100 mbar inlet choke setting after adding surfactant can thus imply that this choke setting creates a significant higher level of water-continuous dispersion compared to the other choke settings. This is indicated by Fig. 11, displaying a thicker water-continuous dispersion for the 100 mbar choke setting.

The overall effect of adding surfactant to the system was negative in terms of separator performance. A decrease in performance was observed for all test points with water dominated inlet conditions, and for the 100 mbar inlet choke configuration for the 30% WC_{in} test points. The decrease in performance is supported by reported droplet size data, displaying a leftward shift in the cumulative plots when surfactant is added and overall lower d_{32} values. This indicates formation of smaller droplets, and because the inlet WC is the same for compared test points, also an increase in the total amount of droplets. This is further supported by the average number of droplets recorded for the surfactant and no-surfactant test points (3457 vs. 2402). Smaller droplets lead to slower separation and hence declined separator performance. Reported IFT for the system did not change after surfactant was added to the Exxsol^{TM} D60, however, an overall decrease in droplet sizes were observed. In addition, the water-continuous dispersion was observed to cause a decline in separator performance, and it is thus believed that the surfactant is causing dispersed Exxsol^{TM} D60 droplets to become more stable.

Connecting reported results to oil–water separation phenomena described in the introduction, a decreased performance with addition of inlet choking and surfactants were to be expected. Increased levels of inlet choking causes dispersed phase break up into smaller droplets (emulsions). Addition of surfactants leads to adsorption of surface-active components on the oil–water interface, stabilizing dispersed oil droplets and hindering droplet coalescence. Reported data are in line with the previous reported results of Fossen et al. (2006), displaying increased emulsion layer thickness with increased levels of inlet choking.

Table A.6
Data and calculated error for fully open $VT.1$, 0 ppm Span®85 tests.

Target values			Recorded values																	
$\dot{Q}_{tot}$	WC_{in}	ER	FT.1 [L/min]		FT.2 [L/min]		FT.3 [L/min]		DT.1 [kg/m^3]		DT.2 [kg/m^3]		DT.3 [kg/m^3]		PT.1 [barg]		dPT.1 [mbar]		TT.1 [°C]	
[L/min]	[%]	[%]	Val	±%	Val	±%	Val	±%	Val	±%	Val	±%	Val	±%	Val	±%	Val	±%	Val	±%
		50	**210,0**	*0,3*	**90,0**	*0,7*	**104,7**	*0,6*	**1020,7**	*0,06*	**795,8**	*0,07*	**1020,6**	*0,06*	**0,21**	*1,7*	**5,0**	*24,4*	**15,6**	*2,1*
	70	**70**	**210,0**	*0,3*	**90,0**	*0,7*	**148,6**	*0,4*	**1020,8**	*0,06*	**795,8**	*0,07*	**1020,6**	*0,06*	**0,21**	*1,7*	**5,2**	*23,2*	**15,6**	*2,1*
		90	**210,0**	*0,3*	**90,0**	*0,7*	**188,1**	*0,4*	**1020,9**	*0,06*	**795,8**	*0,07*	**1020,6**	*0,06*	**0,20**	*1,8*	**5,0**	*24,3*	**15,6**	*2,1*
		50	**150,0**	*0,4*	**150,0**	*0,4*	**76,4**	*0,8*	**1020,8**	*0,06*	**795,7**	*0,07*	**1020,7**	*0,06*	**0,22**	*1,7*	**4,9**	*24,5*	**15,5**	*2,1*
300	**50**	**70**	**150,2**	*0,4*	**150,3**	*0,4*	**103,8**	*0,6*	**1020,8**	*0,06*	**795,7**	*0,07*	**1020,7**	*0,06*	**0,23**	*1,7*	**5,0**	*24,0*	**15,5**	*2,1*
		90	**150,0**	*0,4*	**150,0**	*0,4*	**136,7**	*0,5*	**1020,9**	*0,06*	**795,8**	*0,07*	**1020,5**	*0,06*	**0,20**	*1,9*	**5,1**	*23,9*	**15,5**	*2,1*
		50	**90,0**	*0,7*	**210,0**	*0,3*	**45,0**	*1,4*	**1021,1**	*0,06*	**796,0**	*0,07*	**1020,8**	*0,06*	**0,19**	*1,9*	**5,4**	*22,4*	**15,4**	*2,1*
	30	**70**	**90,0**	*0,7*	**210,0**	*0,3*	**62,5**	*1,0*	**1021,1**	*0,06*	**795,9**	*0,07*	**1020,7**	*0,06*	**0,22**	*1,7*	**4,8**	*24,9*	**15,4**	*2,1*
		90	**90,0**	*0,7*	**210,0**	*0,3*	**80,9**	*0,8*	**1021,0**	*0,06*	**796,0**	*0,07*	**1019,2**	*0,06*	**0,22**	*1,7*	**4,9**	*24,4*	**15,4**	*2,1*
		50	**280,0**	*0,3*	**120,0**	*0,5*	**142,1**	*0,5*	**1020,1**	*0,06*	**795,4**	*0,07*	**1020,0**	*0,06*	**0,19**	*1,9*	**5,0**	*24,0*	**16,0**	*2,0*
	70	**70**	**280,0**	*0,3*	**120,0**	*0,5*	**197,1**	*0,3*	**1020,5**	*0,06*	**795,4**	*0,07*	**1020,2**	*0,06*	**0,21**	*1,7*	**5,0**	*24,2*	**16,0**	*2,0*
		90	**280,0**	*0,3*	**120,0**	*0,5*	**252,8**	*0,3*	**1020,5**	*0,06*	**795,4**	*0,07*	**1019,7**	*0,06*	**0,25**	*1,5*	**4,7**	*25,9*	**16,0**	*2,0*
		50	**200,0**	*0,3*	**200,0**	*0,3*	**100,8**	*0,6*	**1020,7**	*0,06*	**795,4**	*0,07*	**1020,5**	*0,06*	**0,25**	*1,5*	**5,5**	*22,0*	**15,9**	*2,0*
400	**50**	**70**	**200,0**	*0,3*	**200,0**	*0,3*	**140,2**	*0,5*	**1020,8**	*0,06*	**795,4**	*0,07*	**1020,5**	*0,06*	**0,22**	*1,6*	**5,1**	*23,4*	**15,9**	*2,0*
		90	**200,0**	*0,3*	**200,0**	*0,3*	**180,2**	*0,4*	**1020,7**	*0,06*	**795,4**	*0,07*	**1019,0**	*0,06*	**0,20**	*1,8*	**5,0**	*24,0*	**15,9**	*2,0*
		50	**120,0**	*0,5*	**280,0**	*0,3*	**59,8**	*1,0*	**1020,9**	*0,06*	**795,6**	*0,07*	**1020,7**	*0,06*	**0,22**	*1,6*	**5,6**	*21,6*	**15,8**	*2,0*
	30	**70**	**120,0**	*0,5*	**280,0**	*0,3*	**83,5**	*0,7*	**1020,8**	*0,06*	**795,6**	*0,07*	**1019,0**	*0,06*	**0,25**	*1,4*	**5,4**	*22,2*	**15,8**	*2,0*
		90	**120,0**	*0,5*	**280,0**	*0,3*	**108,4**	*0,6*	**1020,6**	*0,06*	**795,6**	*0,07*	**1014,7**	*0,06*	**0,21**	*1,7*	**5,5**	*21,8*	**15,8**	*2,0*
		50	**350,0**	*0,2*	**150,0**	*0,4*	**175,4**	*0,4*	**1018,6**	*0,06*	**795,1**	*0,07*	**1018,4**	*0,06*	**0,22**	*1,6*	**5,4**	*22,4*	**16,1**	*2,0*
	70	**70**	**350,0**	*0,2*	**150,0**	*0,4*	**245,9**	*0,3*	**1019,8**	*0,06*	**795,1**	*0,07*	**1018,7**	*0,06*	**0,21**	*1,7*	**5,4**	*22,4*	**16,2**	*2,0*
		90	**350,0**	*0,2*	**150,0**	*0,4*	**316,7**	*0,3*	**1020,0**	*0,06*	**795,2**	*0,07*	**1016,6**	*0,06*	**0,22**	*1,7*	**5,2**	*23,0*	**16,3**	*2,0*
		50	**250,0**	*0,3*	**250,0**	*0,3*	**124,8**	*0,5*	**1020,6**	*0,06*	**795,9**	*0,07*	**1019,9**	*0,06*	**0,27**	*1,3*	**6,1**	*19,8*	**16,0**	*2,0*
500	**50**	**70**	**250,0**	*0,3*	**250,0**	*0,3*	**174,9**	*0,4*	**1020,4**	*0,06*	**795,3**	*0,07*	**1016,2**	*0,06*	**0,20**	*1,8*	**5,4**	*22,5*	**16,0**	*2,0*
		90	**250,0**	*0,3*	**250,0**	*0,3*	**225,3**	*0,3*	**1019,4**	*0,06*	**795,3**	*0,07*	**999,3**	*0,06*	**0,21**	*1,8*	**5,2**	*23,4*	**16,1**	*2,0*
		50	**150,0**	*0,4*	**350,0**	*0,2*	**75,2**	*0,8*	**1020,7**	*0,06*	**795,5**	*0,07*	**1017,8**	*0,06*	**0,29**	*1,3*	**6,7**	*18,1*	**15,9**	*2,0*
	30	**70**	**150,0**	*0,4*	**350,0**	*0,2*	**106,0**	*0,6*	**1020,5**	*0,06*	**795,6**	*0,07*	**1011,0**	*0,06*	**0,24**	*1,5*	**5,8**	*20,7*	**15,9**	*2,0*
		90	**150,0**	*0,4*	**350,0**	*0,2*	**134,8**	*0,5*	**1020,3**	*0,06*	**795,6**	*0,07*	**1002,0**	*0,06*	**0,19**	*1,9*	**6,3**	*19,3*	**15,9**	*2,0*

Results can be further connected to the use of subsea produced water separators, and the associated potential gain in separator performance. As discussed in the introduction, turbulence, mixing and agitation associated with topside transportation is a cause for oil–water dispersion formation in offshore oil and gas production. The inclusion of choke valves creates further mixing and dispersed phase breakup. The surface-active components present in crude oil systems will over time migrate to the oil water interface, making formed droplets stable and difficult to separate. If separation of oil and water can be done close to the wellhead, the level of mixing will be minimized. In addition, the amount of time passing from droplet formation to separation will be greatly reduced, limiting the amount of migrated surface-active components to the oil water interface. This creates easier separation conditions, which together with already preferential circumstances (lower liquid and emulsion viscosities and larger oil–water density differences) makes the application of subsea produced water separators attractive (Bringedal et al., 1999).

4. Conclusion

This paper has studied the effect of inlet choking and the addition of surfactant on separator performance. The overall trend indicates that separation efficiency is worse with increased levels of inlet choking, and further decreased by the addition of surfactant. These two factors generally lead to an increased dispersion layer thickness at the separator outlet, which was then extracted at higher extraction rates.

For select test points, moderate choking or addition of surfactant lead to a slight increase in recorded performance. This is observed for oil-dominated inlet regimes, and is believed to be caused by a greater number of dispersed water droplets being formed, which could increase coalescence rate.

While the addition of surfactant had an effect on the droplet size distributions, it also became clear that process variables has an equal if not greater effect on the distributions.

Water-continuous inlet regimes can be expected for late life oilfields. For water-continuous inlet regimes, the maximum reduction in calculated WC_r due to inlet choking was recorded at a total flow rate of 500 L/min, for an inlet WC of 50%, being 14 pp. This is also the point with the largest decrease in WC_r due to the addition of surfactant, 4 pp. The maximum reduction in WC_r due to inlet choking and the addition of surfactant was 16 pp compared to the no-choke, no-surfactant case. The addition of surfactant is thus seen to enhance the degradation in performance, especially in combination with inlet choking, for the studied system. It can thus be argued that limiting inlet choking upstream oil–water separators will benefit separation, and that subsea separation is to be preferred, as the conditions for separation are improved the closer you get to the wellhead.

Declaration of competing interest

The authors declare that they have no known competing financial interests or personal relationships that could have appeared to influence the work reported in this paper.

Acknowledgements

This work was carried out as a part of SUBPRO, a Research-based Innovation Centre within Subsea Production and Processing. The authors gratefully acknowledge the financial support from SUBPRO, which is financed by the Research Council of Norway, major industry partners and the Norwegian University of Science and Technology (NTNU), and the Department of Geoscience and Petroleum, NTNU. The authors would also like to thank the Department of Energy and Process Engineering at NTNU, especially Professor Ole Jørgen Nydal, for the loan of the PVM equipment used in this study.

Appendix. Supplementary data

See Tables A.6–A.12 and Figs. A.17–A.25.

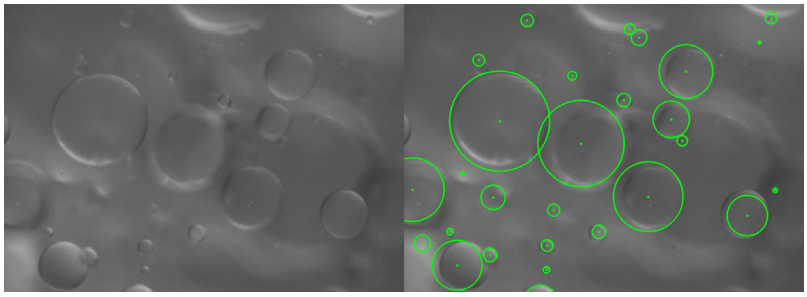

Fig. A.17. Picture of droplet tracking in the automatic counting procedure.

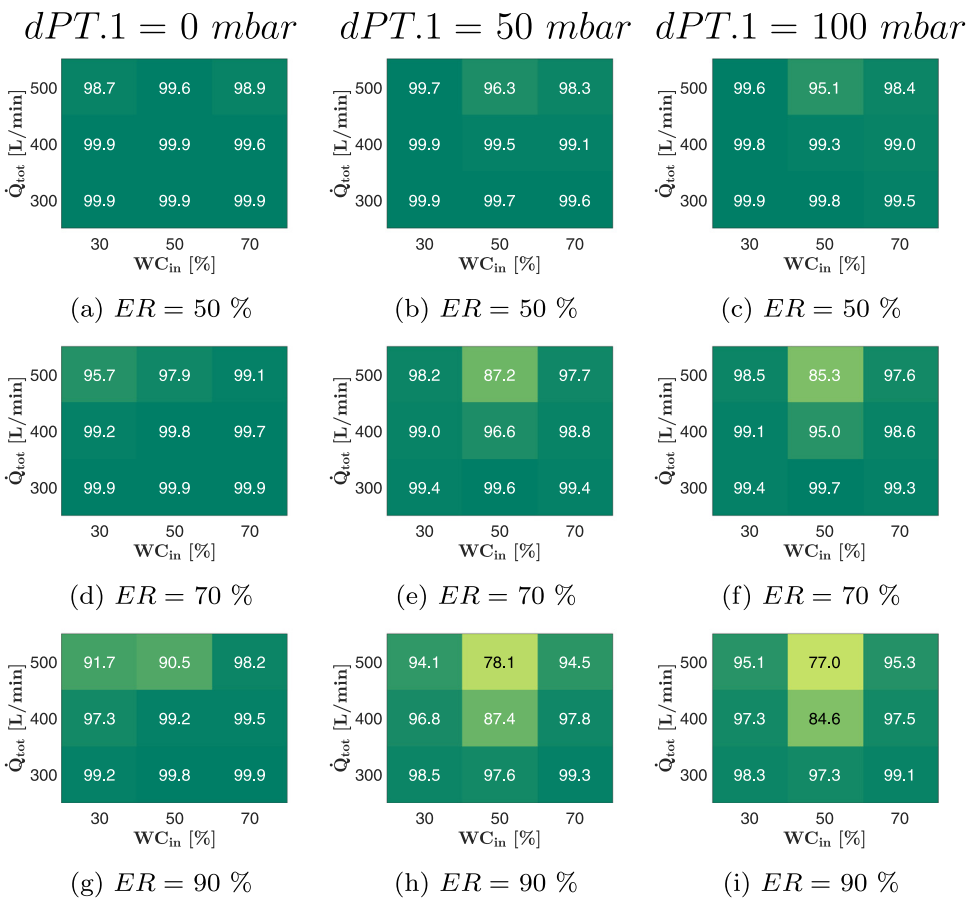

Fig. A.18. WC_3 [%] results for $dPT.1 = 0$, 50, 100 mbar and $ER = 50$, 70, 90% for the no surfactant tests.

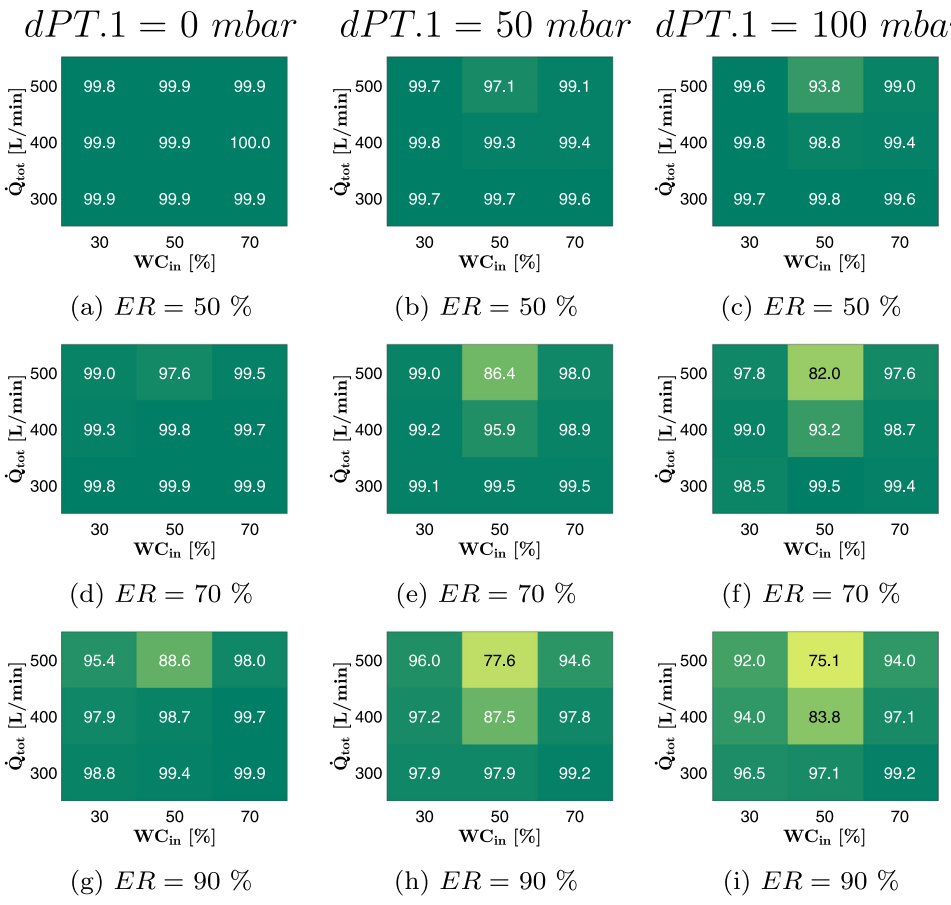

Fig. A.19. WC_r [%] results for $dPT.1 = 0$, 50, 100 mbar and $ER = 50$, 70, 90% for the 15 ppm Span®85 surfactant tests.

Table A.7
Data and calculated error for $dPT.1 = 50$ mbar, 0 ppm Span®85 tests.

Target values			Recorded values																	
$\dot{Q}_{tot}$	WC_{in}	ER	FT.1 [L/min]		FT.2 [L/min]		FT.3 [L/min]		DT.1 [kg/m^3]		DT.2 [kg/m^3]		DT.3 [kg/m^3]		PT.1 [barg]		dPT.1 [mbar]		TT.1 [°C]	
[L/min]	[%]	[%]	Val	±%	Val	±%	Val	±%	Val	±%	Val	±%	Val	±%	Val	±%	Val	±%	Val	±%
		50	**210,0**	*0,3*	**90,0**	*0,7*	**104,8**	*0,6*	**1020,8**	*0,06*	**796,8**	*0,07*	**1020,2**	*0,06*	**0,16**	*2,2*	**49,3**	*2,4*	**14,2**	*2,3*
	70	**70**	**210,0**	*0,3*	**90,0**	*0,7*	**146,1**	*0,4*	**1020,9**	*0,06*	**796,8**	*0,07*	**1020,0**	*0,06*	**0,18**	*2,1*	**48,8**	*2,5*	**14,2**	*2,3*
		90	**210,0**	*0,3*	**90,0**	*0,7*	**188,6**	*0,4*	**1020,8**	*0,06*	**796,8**	*0,07*	**1019,5**	*0,06*	**0,18**	*2,0*	**48,4**	*2,5*	**14,3**	*2,2*
		50	**150,0**	*0,4*	**150,0**	*0,4*	**74,7**	*0,8*	**1021,1**	*0,06*	**796,8**	*0,07*	**1020,6**	*0,06*	**0,18**	*2,0*	**50,3**	*2,4*	**14,0**	*2,3*
300	**50**	**70**	**150,0**	*0,4*	**150,0**	*0,4*	**103,8**	*0,6*	**1021,0**	*0,06*	**796,8**	*0,07*	**1020,3**	*0,06*	**0,13**	*2,9*	**51,1**	*2,4*	**14,1**	*2,3*
		90	**150,0**	*0,4*	**150,0**	*0,4*	**134,3**	*0,5*	**1020,7**	*0,06*	**796,9**	*0,07*	**1015,9**	*0,06*	**0,26**	*1,4*	**52,9**	*2,3*	**14,1**	*2,3*
		50	**90,0**	*0,7*	**210,0**	*0,3*	**46,0**	*1,3*	**1021,3**	*0,06*	**797,0**	*0,07*	**1021,1**	*0,06*	**0,23**	*1,5*	**51,4**	*2,3*	**14,0**	*2,3*
	30	**70**	**90,0**	*0,7*	**210,0**	*0,3*	**64,1**	*1,0*	**1021,3**	*0,06*	**797,0**	*0,07*	**1020,0**	*0,06*	**0,22**	*1,7*	**50,8**	*2,4*	**14,0**	*2,3*
		90	**90,0**	*0,7*	**210,0**	*0,3*	**81,8**	*0,8*	**1021,1**	*0,06*	**797,1**	*0,07*	**1017,9**	*0,06*	**0,17**	*2,2*	**50,1**	*2,4*	**14,0**	*2,3*
		50	**280,0**	*0,3*	**120,0**	*0,5*	**139,8**	*0,5*	**1020,0**	*0,06*	**796,1**	*0,07*	**1019,1**	*0,06*	**0,22**	*1,7*	**49,9**	*2,4*	**14,7**	*2,2*
	70	**70**	**280,0**	*0,3*	**120,0**	*0,5*	**195,1**	*0,3*	**1020,4**	*0,06*	**796,2**	*0,07*	**1018,4**	*0,06*	**0,15**	*2,3*	**50,3**	*2,4*	**14,8**	*2,2*
		90	**280,0**	*0,3*	**120,0**	*0,5*	**251,3**	*0,3*	**1020,3**	*0,06*	**796,2**	*0,07*	**1016,0**	*0,06*	**0,21**	*1,7*	**49,7**	*2,4*	**14,8**	*2,2*
		50	**200,0**	*0,3*	**200,0**	*0,3*	**100,2**	*0,6*	**1020,5**	*0,06*	**796,2**	*0,07*	**1020,0**	*0,06*	**0,21**	*1,7*	**51,5**	*2,3*	**14,6**	*2,2*
400	**50**	**70**	**200,0**	*0,3*	**200,0**	*0,3*	**140,6**	*0,5*	**1020,6**	*0,06*	**796,2**	*0,07*	**1013,4**	*0,06*	**0,23**	*1,6*	**50,8**	*2,4*	**14,6**	*2,2*
		90	**200,0**	*0,3*	**200,0**	*0,3*	**180,5**	*0,4*	**1020,3**	*0,06*	**796,4**	*0,07*	**992,7**	*0,07*	**0,21**	*1,8*	**50,6**	*2,4*	**14,6**	*2,2*
		50	**120,0**	*0,5*	**280,0**	*0,3*	**60,1**	*1,0*	**1021,2**	*0,06*	**796,6**	*0,07*	**1020,9**	*0,06*	**0,20**	*1,9*	**49,3**	*2,4*	**14,4**	*2,2*
	30	**70**	**120,0**	*0,5*	**280,0**	*0,3*	**84,4**	*0,7*	**1021,1**	*0,06*	**796,6**	*0,07*	**1018,9**	*0,06*	**0,18**	*2,0*	**49,3**	*2,4*	**14,4**	*2,2*
		90	**120,0**	*0,5*	**280,0**	*0,3*	**108,3**	*0,6*	**1020,9**	*0,06*	**796,6**	*0,07*	**1014,1**	*0,06*	**0,16**	*2,3*	**49,7**	*2,4*	**14,4**	*2,2*
		50	**350,0**	*0,2*	**150,0**	*0,4*	**173,8**	*0,4*	**1018,9**	*0,06*	**795,8**	*0,07*	**1017,3**	*0,06*	**0,21**	*1,7*	**51,9**	*2,3*	**15,1**	*2,1*
	70	**70**	**350,0**	*0,2*	**150,0**	*0,4*	**243,7**	*0,3*	**1019,8**	*0,06*	**795,8**	*0,07*	**1015,8**	*0,06*	**0,17**	*2,1*	**51,7**	*2,3*	**15,1**	*2,1*
		90	**350,0**	*0,2*	**150,0**	*0,4*	**316,6**	*0,2*	**1019,7**	*0,06*	**795,8**	*0,07*	**1008,6**	*0,06*	**0,19**	*2,0*	**52,2**	*2,3*	**15,2**	*2,1*
		50	**250,0**	*0,3*	**250,0**	*0,3*	**125,0**	*0,5*	**1019,0**	*0,06*	**795,9**	*0,07*	**1012,7**	*0,06*	**0,28**	*1,3*	**49,6**	*2,4*	**15,0**	*2,1*
500	**50**	**70**	**250,0**	*0,3*	**250,0**	*0,3*	**174,6**	*0,4*	**1019,3**	*0,06*	**795,9**	*0,07*	**992,2**	*0,06*	**0,21**	*1,7*	**50,1**	*2,4*	**15,0**	*2,1*
		90	**250,0**	*0,3*	**250,0**	*0,3*	**226,0**	*0,3*	**1019,5**	*0,06*	**795,9**	*0,07*	**971,7**	*0,07*	**0,21**	*1,7*	**49,5**	*2,4*	**15,1**	*2,1*
		50	**150,0**	*0,4*	**350,0**	*0,2*	**75,5**	*0,8*	**1020,9**	*0,06*	**796,5**	*0,07*	**1020,4**	*0,06*	**0,29**	*1,3*	**48,4**	*2,5*	**14,9**	*2,1*
	30	**70**	**150,0**	*0,4*	**350,0**	*0,2*	**104,6**	*0,6*	**1020,9**	*0,06*	**796,3**	*0,07*	**1016,9**	*0,06*	**0,24**	*1,5*	**48,3**	*2,5*	**14,9**	*2,1*
		90	**150,0**	*0,4*	**350,0**	*0,2*	**135,0**	*0,5*	**1020,6**	*0,06*	**796,4**	*0,07*	**1007,7**	*0,06*	**0,20**	*1,8*	**49,0**	*2,5*	**15,0**	*2,1*

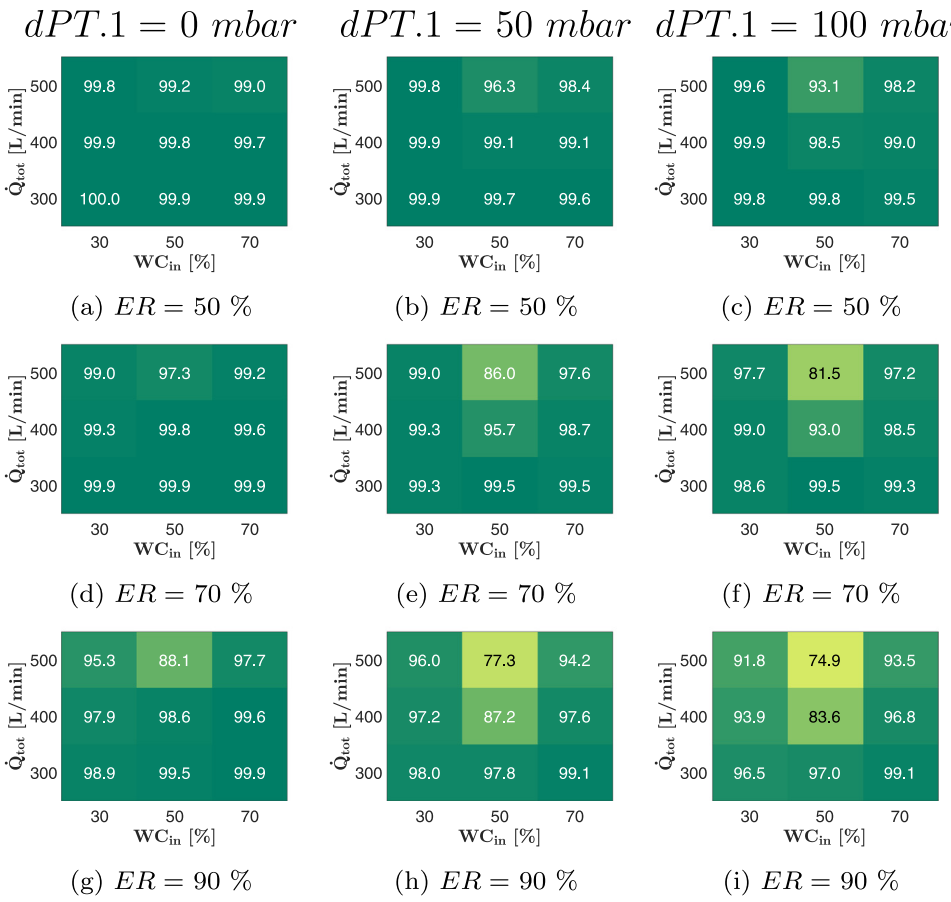

Fig. A.20. WC_3 [%] results for $dPT.1 = 0$, 50, 100 mbar and $ER = 50$, 70, 90% for the 15 ppm Span®85 surfactant tests.

Table A.8
Data and calculated error for $dPT.1 = 100$ mbar, 0 ppm Span®85 tests.

Target values			Recorded values																	
$\dot{Q}_{tot}$	WC_{in}	ER	FT.1 [L/min]		FT.2 [L/min]		FT.3 [L/min]		DT.1 [kg/m^3]		DT.2 [kg/m^3]		DT.3 [kg/m^3]		PT.1 [barg]		dPT.1 [mbar]		TT.1 [°C]	
[L/min]	[%]	[%]	Val	±%	Val	±%	Val	±%	Val	±%	Val	±%	Val	±%	Val	±%	Val	±%	Val	±%
		50	**210,0**	*0,3*	**90,0**	*0,7*	**104,3**	*0,6*	**1020,6**	*0,06*	**796,4**	*0,07*	**1019,9**	*0,06*	**0,27**	*1,3*	**100,9**	*1,2*	**14,9**	*2,1*
	70	**70**	**210,0**	*0,3*	**90,0**	*0,7*	**148,6**	*0,4*	**1020,6**	*0,06*	**796,4**	*0,07*	**1019,6**	*0,06*	**0,27**	*1,3*	**101,1**	*1,2*	**14,9**	*2,1*
		90	**210,0**	*0,3*	**90,0**	*0,7*	**189,8**	*0,4*	**1020,6**	*0,06*	**796,4**	*0,07*	**1018,9**	*0,06*	**0,23**	*1,6*	**100,0**	*1,2*	**15,0**	*2,1*
		50	**150,0**	*0,4*	**150,0**	*0,4*	**74,8**	*0,8*	**1020,9**	*0,06*	**796,2**	*0,07*	**1020,6**	*0,06*	**0,26**	*1,4*	**99,6**	*1,2*	**14,8**	*2,2*
300	**50**	**70**	**150,1**	*0,4*	**150,1**	*0,4*	**105,5**	*0,6*	**1020,9**	*0,06*	**796,2**	*0,07*	**1020,5**	*0,06*	**0,21**	*1,8*	**99,7**	*1,2*	**14,8**	*2,2*
		90	**150,0**	*0,4*	**150,0**	*0,4*	**135,8**	*0,5*	**1020,7**	*0,06*	**796,3**	*0,07*	**1014,9**	*0,06*	**0,21**	*1,7*	**100,3**	*1,2*	**14,9**	*2,2*
		50	**90,0**	*0,7*	**210,0**	*0,3*	**45,8**	*1,3*	**1021,1**	*0,06*	**796,4**	*0,07*	**1020,9**	*0,06*	**0,20**	*1,9*	**100,3**	*1,2*	**14,7**	*2,2*
	30	**70**	**90,0**	*0,7*	**210,0**	*0,3*	**63,1**	*1,0*	**1021,1**	*0,06*	**796,5**	*0,07*	**1019,7**	*0,06*	**0,17**	*2,1*	**100,6**	*1,2*	**14,7**	*2,2*
		90	**90,0**	*0,7*	**210,0**	*0,3*	**81,5**	*0,8*	**1021,0**	*0,06*	**796,5**	*0,07*	**1017,4**	*0,06*	**0,23**	*1,6*	**100,3**	*1,2*	**14,8**	*2,2*
		50	**280,0**	*0,3*	**120,0**	*0,5*	**140,3**	*0,5*	**1019,8**	*0,06*	**795,7**	*0,07*	**1018,8**	*0,06*	**0,28**	*1,3*	**98,9**	*1,2*	**15,4**	*2,1*
	70	**70**	**280,0**	*0,3*	**120,0**	*0,5*	**195,0**	*0,3*	**1020,2**	*0,06*	**795,8**	*0,07*	**1017,8**	*0,06*	**0,18**	*2,0*	**99,8**	*1,2*	**15,4**	*2,1*
		90	**280,0**	*0,3*	**120,0**	*0,5*	**252,5**	*0,3*	**1020,1**	*0,06*	**795,8**	*0,07*	**1015,4**	*0,06*	**0,27**	*1,4*	**99,5**	*1,2*	**15,4**	*2,1*
		50	**200,0**	*0,3*	**200,0**	*0,3*	**100,0**	*0,6*	**1020,2**	*0,06*	**795,9**	*0,07*	**1019,4**	*0,06*	**0,26**	*1,4*	**98,3**	*1,2*	**15,3**	*2,1*
400	**50**	**70**	**200,0**	*0,3*	**200,0**	*0,3*	**141,1**	*0,5*	**1020,4**	*0,06*	**795,8**	*0,07*	**1009,7**	*0,06*	**0,21**	*1,7*	**99,4**	*1,2*	**15,3**	*2,1*
		90	**200,0**	*0,3*	**200,0**	*0,3*	**182,5**	*0,4*	**1020,1**	*0,06*	**795,9**	*0,07*	**986,3**	*0,07*	**0,29**	*1,3*	**98,8**	*1,2*	**15,3**	*2,1*
		50	**120,0**	*0,5*	**280,0**	*0,3*	**59,5**	*1,0*	**1021,0**	*0,06*	**796,3**	*0,07*	**1020,6**	*0,06*	**0,17**	*2,2*	**99,8**	*1,2*	**15,1**	*2,1*
	30	**70**	**120,0**	*0,5*	**280,0**	*0,3*	**84,7**	*0,7*	**1020,9**	*0,06*	**796,1**	*0,07*	**1018,9**	*0,06*	**0,18**	*2,0*	**99,8**	*1,2*	**15,1**	*2,1*
		90	**120,0**	*0,5*	**280,0**	*0,3*	**107,7**	*0,6*	**1020,7**	*0,06*	**796,1**	*0,07*	**1015,0**	*0,06*	**0,21**	*1,8*	**98,8**	*1,2*	**15,1**	*2,1*
		50	**350,0**	*0,2*	**150,0**	*0,4*	**175,4**	*0,4*	**1018,8**	*0,06*	**795,2**	*0,07*	**1017,1**	*0,06*	**0,27**	*1,3*	**101,7**	*1,2*	**16,0**	*2,0*
	70	**70**	**350,0**	*0,2*	**150,0**	*0,4*	**244,8**	*0,3*	**1019,5**	*0,06*	**795,2**	*0,07*	**1015,5**	*0,06*	**0,24**	*1,5*	**102,0**	*1,2*	**16,0**	*2,0*
		90	**350,0**	*0,2*	**150,0**	*0,4*	**314,0**	*0,2*	**1019,5**	*0,06*	**795,2**	*0,07*	**1010,3**	*0,06*	**0,25**	*1,5*	**101,9**	*1,2*	**16,0**	*2,0*
		50	**250,0**	*0,3*	**250,0**	*0,3*	**126,2**	*0,5*	**1019,0**	*0,06*	**795,4**	*0,07*	**1009,8**	*0,06*	**0,30**	*1,2*	**99,3**	*1,2*	**15,8**	*2,0*
500	**50**	**70**	**250,0**	*0,3*	**250,0**	*0,3*	**176,9**	*0,4*	**1019,4**	*0,06*	**795,4**	*0,07*	**987,8**	*0,06*	**0,22**	*1,7*	**100,3**	*1,2*	**15,8**	*2,0*
		90	**250,0**	*0,3*	**250,0**	*0,3*	**226,0**	*0,3*	**1019,7**	*0,06*	**795,4**	*0,07*	**968,9**	*0,07*	**0,22**	*1,7*	**100,2**	*1,2*	**15,8**	*2,0*
		50	**150,0**	*0,4*	**350,0**	*0,2*	**74,4**	*0,8*	**1020,8**	*0,06*	**796,1**	*0,07*	**1020,0**	*0,06*	**0,30**	*1,2*	**98,8**	*1,2*	**15,6**	*2,1*
	30	**70**	**150,0**	*0,4*	**350,0**	*0,2*	**104,9**	*0,6*	**1020,8**	*0,06*	**795,9**	*0,07*	**1017,6**	*0,06*	**0,24**	*1,5*	**97,7**	*1,2*	**15,6**	*2,1*
		90	**150,0**	*0,4*	**350,0**	*0,2*	**135,3**	*0,5*	**1020,5**	*0,06*	**795,8**	*0,07*	**1009,8**	*0,06*	**0,25**	*1,5*	**98,3**	*1,2*	**15,7**	*2,0*

Table A.9
Data and calculated error for fully open $VT.1$, 15 ppm Span®85 tests.

Target values			Recorded values																	
$\dot{Q}_{tot}$	WC_{in}	ER	FT.1 [L/min]		FT.2 [L/min]		FT.3 [L/min]		DT.1 [kg/m^3]		DT.2 [kg/m^3]		DT.3 [kg/m^3]		PT.1 [barg]		dPT.1 [mbar]		TT.1 [°C]	
[L/min]	[%]	[%]	Val	±%	Val	±%	Val	±%	Val	±%	Val	±%	Val	±%	Val	±%	Val	±%	Val	±%
		50	**210,0**	*0,3*	**90,0**	*0,7*	**105,1**	*0,6*	**1020,6**	*0,06*	**795,1**	*0,07*	**1020,4**	*0,06*	**0,24**	*1,5*	**2,6**	*46,3*	**16,7**	*1,9*
	70	**70**	**210,0**	*0,3*	**90,0**	*0,7*	**147,3**	*0,4*	**1020,7**	*0,06*	**795,2**	*0,07*	**1020,4**	*0,06*	**0,18**	*2,0*	**2,7**	*45,4*	**16,7**	*1,9*
		90	**210,0**	*0,3*	**90,0**	*0,7*	**190,3**	*0,4*	**1020,7**	*0,06*	**795,1**	*0,07*	**1020,4**	*0,06*	**0,25**	*1,5*	**2,9**	*42,1*	**16,7**	*1,9*
		50	**150,0**	*0,4*	**150,0**	*0,4*	**75,1**	*0,8*	**1020,8**	*0,06*	**795,0**	*0,07*	**1020,5**	*0,06*	**0,20**	*1,8*	**2,6**	*45,6*	**16,6**	*1,9*
300	**50**	**70**	**150,0**	*0,4*	**150,0**	*0,4*	**106,0**	*0,6*	**1020,7**	*0,06*	**795,0**	*0,07*	**1020,5**	*0,06*	**0,33**	*1,1*	**2,2**	*53,7*	**16,6**	*1,9*
		90	**150,0**	*0,4*	**150,0**	*0,4*	**136,1**	*0,5*	**1020,7**	*0,06*	**795,1**	*0,07*	**1019,4**	*0,06*	**0,18**	*2,0*	**2,3**	*52,1*	**16,7**	*1,9*
		50	**90,0**	*0,7*	**210,0**	*0,3*	**44,5**	*1,4*	**1020,9**	*0,06*	**795,2**	*0,07*	**1020,6**	*0,06*	**0,21**	*1,7*	**2,8**	*42,4*	**16,6**	*1,9*
	30	**70**	**90,0**	*0,7*	**210,0**	*0,3*	**62,8**	*1,0*	**1020,8**	*0,06*	**795,2**	*0,07*	**1020,4**	*0,06*	**0,26**	*1,4*	**2,6**	*46,7*	**16,6**	*1,9*
		90	**90,0**	*0,7*	**210,0**	*0,3*	**81,2**	*0,8*	**1020,8**	*0,06*	**795,2**	*0,07*	**1018,2**	*0,06*	**0,19**	*2,0*	**2,5**	*48,3*	**16,6**	*1,9*
		50	**280,0**	*0,3*	**120,0**	*0,5*	**141,6**	*0,5*	**1019,9**	*0,06*	**794,8**	*0,07*	**1019,8**	*0,06*	**0,24**	*1,5*	**2,7**	*44,0*	**17,0**	*1,9*
	70	**70**	**280,0**	*0,3*	**120,0**	*0,5*	**197,6**	*0,3*	**1020,3**	*0,06*	**794,8**	*0,07*	**1019,6**	*0,06*	**0,21**	*1,7*	**2,7**	*44,9*	**17,0**	*1,9*
		90	**280,0**	*0,3*	**120,0**	*0,5*	**253,7**	*0,3*	**1020,4**	*0,06*	**794,8**	*0,07*	**1019,7**	*0,06*	**0,21**	*1,7*	**2,0**	*60,3*	**17,0**	*1,9*
		50	**200,0**	*0,3*	**200,0**	*0,3*	**100,6**	*0,6*	**1020,4**	*0,06*	**794,8**	*0,07*	**1020,3**	*0,06*	**0,22**	*1,7*	**2,8**	*43,7*	**16,8**	*1,9*
400	**50**	**70**	**200,0**	*0,3*	**200,0**	*0,3*	**140,4**	*0,5*	**1020,6**	*0,06*	**794,8**	*0,07*	**1020,2**	*0,06*	**0,23**	*1,6*	**2,9**	*41,7*	**16,9**	*1,9*
		90	**200,0**	*0,3*	**200,0**	*0,3*	**179,9**	*0,4*	**1020,5**	*0,06*	**794,9**	*0,07*	**1017,5**	*0,06*	**0,21**	*1,7*	**2,7**	*44,3*	**16,9**	*1,9*
		50	**120,0**	*0,5*	**280,0**	*0,3*	**59,9**	*1,0*	**1020,7**	*0,06*	**795,1**	*0,07*	**1020,5**	*0,06*	**0,22**	*1,7*	**2,7**	*45,3*	**16,8**	*1,9*
	30	**70**	**120,0**	*0,5*	**280,0**	*0,3*	**84,2**	*0,7*	**1020,7**	*0,06*	**795,0**	*0,07*	**1019,1**	*0,06*	**0,18**	*2,0*	**2,7**	*44,6*	**16,8**	*1,9*
		90	**120,0**	*0,5*	**280,0**	*0,3*	**107,6**	*0,6*	**1020,6**	*0,06*	**794,9**	*0,07*	**1015,8**	*0,06*	**0,21**	*1,7*	**2,7**	*44,9*	**16,8**	*1,9*
		50	**350,0**	*0,2*	**150,0**	*0,4*	**175,2**	*0,4*	**1018,5**	*0,06*	**794,3**	*0,07*	**1018,3**	*0,06*	**0,25**	*1,5*	**2,0**	*61,1*	**17,3**	*1,8*
	70	**70**	**350,0**	*0,2*	**150,0**	*0,4*	**245,4**	*0,3*	**1019,7**	*0,06*	**794,3**	*0,07*	**1018,7**	*0,06*	**0,19**	*1,9*	**1,9**	*65,0*	**17,3**	*1,8*
		90	**350,0**	*0,2*	**150,0**	*0,4*	**315,2**	*0,2*	**1019,8**	*0,06*	**794,3**	*0,07*	**1015,2**	*0,06*	**0,22**	*1,7*	**2,2**	*55,7*	**17,3**	*1,8*
		50	**250,0**	*0,3*	**250,0**	*0,3*	**125,2**	*0,5*	**1019,0**	*0,06*	**794,3**	*0,07*	**1018,7**	*0,06*	**0,27**	*1,4*	**2,8**	*43,8*	**17,2**	*1,9*
500	**50**	**70**	**250,0**	*0,3*	**250,0**	*0,3*	**174,7**	*0,4*	**1019,9**	*0,06*	**794,5**	*0,07*	**1014,4**	*0,06*	**0,22**	*1,6*	**2,7**	*44,7*	**17,2**	*1,9*
		90	**250,0**	*0,3*	**250,1**	*0,3*	**225,1**	*0,3*	**1019,2**	*0,06*	**794,5**	*0,07*	**993,5**	*0,07*	**0,23**	*1,6*	**1,7**	*70,3*	**17,2**	*1,9*
		50	**150,0**	*0,4*	**350,0**	*0,2*	**74,9**	*0,8*	**1020,5**	*0,06*	**794,9**	*0,07*	**1020,2**	*0,06*	**0,31**	*1,2*	**3,3**	*36,6*	**17,1**	*1,9*
	30	**70**	**150,0**	*0,4*	**350,0**	*0,2*	**105,3**	*0,6*	**1020,5**	*0,06*	**794,8**	*0,07*	**1018,3**	*0,06*	**0,26**	*1,4*	**3,5**	*34,8*	**17,1**	*1,9*
		90	**150,0**	*0,4*	**350,0**	*0,2*	**135,0**	*0,5*	**1020,4**	*0,06*	**794,8**	*0,07*	**1009,9**	*0,06*	**0,21**	*1,7*	**2,8**	*42,4*	**17,1**	*1,9*

Table A.10
Data and calculated error for $dPT.1 = 50$ mbar, 15 ppm Span®85 tests.

Target values			Recorded values																	
$\dot{Q}_{tot}$	WC_{in}	ER	FT.1 [L/min]		FT.2 [L/min]		FT.3 [L/min]		DT.1 [kg/m^3]		DT.2 [kg/m^3]		DT.3 [kg/m^3]		PT.1 [barg]		dPT.1 [mbar]		TT.1 [°C]	
[L/min]	[%]	[%]	Val	±%	Val	±%	Val	±%	Val	±%	Val	±%	Val	±%	Val	±%	Val	±%	Val	±%
		50	**210,0**	*0,3*	**90,0**	*0,7*	**104,5**	*0,6*	**1020,5**	*0,06*	**795,3**	*0,07*	**1019,7**	*0,06*	**0,28**	*1,3*	**50,2**	*2,4*	**16,7**	*1,9*
	70	**70**	**210,0**	*0,3*	**90,0**	*0,7*	**146,4**	*0,4*	**1020,6**	*0,06*	**795,4**	*0,07*	**1019,4**	*0,06*	**0,19**	*1,9*	**48,4**	*2,5*	**16,7**	*1,9*
		90	**210,0**	*0,3*	**90,0**	*0,7*	**189,5**	*0,4*	**1020,5**	*0,06*	**795,3**	*0,07*	**1018,6**	*0,06*	**0,24**	*1,5*	**49,7**	*2,4*	**16,7**	*1,9*
		50	**150,0**	*0,4*	**150,0**	*0,4*	**75,0**	*0,8*	**1020,8**	*0,06*	**795,2**	*0,07*	**1020,1**	*0,06*	**0,22**	*1,7*	**49,2**	*2,5*	**16,6**	*1,9*
300	**50**	**70**	**150,0**	*0,4*	**150,0**	*0,4*	**105,8**	*0,6*	**1020,8**	*0,06*	**795,2**	*0,07*	**1019,6**	*0,06*	**0,19**	*2,0*	**49,2**	*2,5*	**16,6**	*1,9*
		90	**150,0**	*0,4*	**150,0**	*0,4*	**134,6**	*0,5*	**1020,6**	*0,06*	**795,3**	*0,07*	**1015,8**	*0,06*	**0,21**	*1,8*	**49,5**	*2,4*	**16,6**	*1,9*
		50	**90,0**	*0,7*	**210,0**	*0,3*	**45,0**	*1,4*	**1021,0**	*0,06*	**795,3**	*0,07*	**1020,3**	*0,06*	**0,22**	*1,7*	**49,9**	*2,4*	**16,6**	*1,9*
	30	**70**	**90,0**	*0,7*	**210,0**	*0,3*	**62,6**	*1,0*	**1021,0**	*0,06*	**795,4**	*0,07*	**1019,0**	*0,06*	**0,17**	*2,1*	**49,8**	*2,4*	**16,6**	*1,9*
		90	**90,0**	*0,7*	**210,0**	*0,3*	**81,3**	*0,8*	**1020,8**	*0,06*	**795,3**	*0,07*	**1016,0**	*0,06*	**0,27**	*1,4*	**51,0**	*2,4*	**16,6**	*1,9*
		50	**280,0**	*0,3*	**120,0**	*0,5*	**139,4**	*0,5*	**1019,8**	*0,06*	**794,8**	*0,07*	**1018,5**	*0,06*	**0,24**	*1,5*	**49,4**	*2,4*	**16,9**	*1,9*
	70	**70**	**280,0**	*0,3*	**120,0**	*0,5*	**197,8**	*0,3*	**1020,1**	*0,06*	**794,7**	*0,07*	**1017,7**	*0,06*	**0,27**	*1,4*	**48,1**	*2,5*	**16,9**	*1,9*
		90	**279,8**	*0,3*	**119,7**	*0,6*	**253,4**	*0,3*	**1020,1**	*0,06*	**794,9**	*0,07*	**1015,1**	*0,06*	**0,25**	*1,5*	**49,5**	*2,4*	**17,0**	*1,9*
		50	**200,0**	*0,3*	**200,0**	*0,3*	**101,1**	*0,6*	**1020,1**	*0,06*	**794,8**	*0,07*	**1018,5**	*0,06*	**0,21**	*1,8*	**51,1**	*2,4*	**16,8**	*1,9*
400	**50**	**70**	**200,0**	*0,3*	**200,0**	*0,3*	**139,9**	*0,5*	**1020,3**	*0,06*	**794,8**	*0,07*	**1011,0**	*0,06*	**0,20**	*1,8*	**52,0**	*2,3*	**16,8**	*1,9*
		90	**200,0**	*0,3*	**200,0**	*0,3*	**179,4**	*0,4*	**1020,0**	*0,06*	**794,9**	*0,07*	**991,7**	*0,07*	**0,26**	*1,4*	**50,6**	*2,4*	**16,8**	*1,9*
		50	**120,0**	*0,5*	**280,0**	*0,3*	**60,5**	*1,0*	**1020,8**	*0,06*	**795,3**	*0,07*	**1020,3**	*0,06*	**0,21**	*1,8*	**50,0**	*2,4*	**16,7**	*1,9*
	30	**70**	**120,0**	*0,5*	**280,0**	*0,3*	**84,9**	*0,7*	**1020,8**	*0,06*	**795,2**	*0,07*	**1019,0**	*0,06*	**0,20**	*1,8*	**50,4**	*2,4*	**16,8**	*1,9*
		90	**120,0**	*0,5*	**280,0**	*0,3*	**108,5**	*0,6*	**1020,6**	*0,06*	**795,1**	*0,07*	**1014,2**	*0,06*	**0,18**	*2,0*	**50,3**	*2,4*	**16,8**	*1,9*
		50	**350,0**	*0,2*	**150,0**	*0,4*	**174,4**	*0,4*	**1018,9**	*0,06*	**794,3**	*0,07*	**1016,9**	*0,06*	**0,22**	*1,6*	**51,5**	*2,3*	**17,3**	*1,9*
	70	**70**	**350,0**	*0,2*	**150,0**	*0,4*	**245,7**	*0,3*	**1019,5**	*0,06*	**794,3**	*0,07*	**1015,1**	*0,06*	**0,19**	*1,9*	**51,8**	*2,3*	**17,3**	*1,8*
		90	**350,0**	*0,2*	**150,0**	*0,4*	**314,3**	*0,2*	**1019,5**	*0,06*	**794,3**	*0,07*	**1007,4**	*0,06*	**0,18**	*2,0*	**52,4**	*2,3*	**17,3**	*1,8*
		50	**250,0**	*0,3*	**250,0**	*0,3*	**125,9**	*0,5*	**1018,6**	*0,06*	**794,5**	*0,07*	**1012,1**	*0,06*	**0,28**	*1,3*	**51,5**	*2,3*	**17,1**	*1,9*
500	**50**	**70**	**250,0**	*0,3*	**250,0**	*0,3*	**175,1**	*0,4*	**1019,4**	*0,06*	**794,4**	*0,07*	**988,8**	*0,06*	**0,23**	*1,6*	**52,3**	*2,3*	**17,2**	*1,9*
		90	**250,0**	*0,3*	**250,0**	*0,3*	**226,8**	*0,3*	**1019,8**	*0,06*	**794,5**	*0,07*	**969,2**	*0,07*	**0,20**	*1,8*	**52,2**	*2,3*	**17,2**	*1,9*
		50	**150,0**	*0,4*	**350,0**	*0,2*	**75,6**	*0,8*	**1020,6**	*0,06*	**795,1**	*0,07*	**1020,0**	*0,06*	**0,30**	*1,2*	**50,2**	*2,4*	**17,1**	*1,9*
	30	**70**	**150,0**	*0,4*	**350,0**	*0,2*	**104,6**	*0,6*	**1020,6**	*0,06*	**795,0**	*0,07*	**1018,3**	*0,06*	**0,25**	*1,5*	**50,0**	*2,4*	**17,1**	*1,9*
		90	**150,0**	*0,4*	**350,0**	*0,2*	**134,7**	*0,5*	**1020,4**	*0,06*	**795,0**	*0,07*	**1011,5**	*0,06*	**0,20**	*1,8*	**50,3**	*2,4*	**17,1**	*1,9*

Table A.11
Data and calculated error for $dPT.1 = 100$ mbar, 15 ppm Span®85 tests.

Target values			Recorded values																	
$\dot{Q}_{tot}$	WC_{in}	ER	FT.1 [L/min]		FT.2 [L/min]		FT.3 [L/min]		DT.1 [kg/m^3]		DT.2 [kg/m^3]		DT.3 [kg/m^3]		PT.1 [barg]		dPT.1 [mbar]		TT.1 [°C]	
[L/min]	[%]	[%]	Val	±%	Val	±%	Val	±%	Val	±%	Val	±%	Val	±%	Val	±%	Val	±%	Val	±%
		50	**210,0**	*0,3*	**90,0**	*0,7*	**106,2**	*0,6*	**1020,4**	*0,06*	**795,4**	*0,07*	**1019,6**	*0,06*	**0,23**	*1,6*	**100,4**	*1,2*	**16,6**	*1,9*
	70	**70**	**210,0**	*0,3*	**90,0**	*0,7*	**149,0**	*0,4*	**1020,5**	*0,06*	**795,3**	*0,07*	**1019,2**	*0,06*	**0,24**	*1,5*	**100,9**	*1,2*	**16,6**	*1,9*
		90	**210,0**	*0,3*	**90,0**	*0,7*	**188,1**	*0,4*	**1020,4**	*0,06*	**795,3**	*0,07*	**1018,5**	*0,06*	**0,17**	*2,1*	**99,7**	*1,2*	**16,6**	*1,9*
		50	**150,0**	*0,4*	**150,0**	*0,4*	**75,4**	*0,8*	**1020,7**	*0,06*	**795,2**	*0,07*	**1020,3**	*0,06*	**0,18**	*2,0*	**99,4**	*1,2*	**16,6**	*1,9*
300	**50**	**70**	**149,9**	*0,4*	**149,9**	*0,4*	**105,8**	*0,6*	**1020,7**	*0,06*	**795,2**	*0,07*	**1019,6**	*0,06*	**0,26**	*1,4*	**100,2**	*1,2*	**16,6**	*1,9*
		90	**150,0**	*0,4*	**150,0**	*0,4*	**135,5**	*0,5*	**1020,5**	*0,06*	**795,3**	*0,07*	**1014,0**	*0,06*	**0,24**	*1,5*	**99,7**	*1,2*	**16,6**	*1,9*
		50	**90,0**	*0,7*	**210,0**	*0,3*	**45,7**	*1,3*	**1020,9**	*0,06*	**795,4**	*0,07*	**1020,3**	*0,06*	**0,25**	*1,5*	**99,1**	*1,2*	**16,5**	*1,9*
	30	**70**	**90,0**	*0,7*	**210,0**	*0,3*	**63,3**	*1,0*	**1020,9**	*0,06*	**795,4**	*0,07*	**1017,6**	*0,06*	**0,20**	*1,8*	**99,0**	*1,2*	**16,5**	*1,9*
		90	**90,0**	*0,7*	**210,0**	*0,3*	**81,4**	*0,8*	**1020,7**	*0,06*	**795,3**	*0,07*	**1012,7**	*0,06*	**0,18**	*2,0*	**98,7**	*1,2*	**16,5**	*1,9*
		50	**280,0**	*0,3*	**120,0**	*0,5*	**139,9**	*0,5*	**1019,8**	*0,06*	**794,7**	*0,07*	**1018,4**	*0,06*	**0,17**	*2,1*	**100,9**	*1,2*	**16,8**	*1,9*
	70	**70**	**280,0**	*0,3*	**120,0**	*0,5*	**197,1**	*0,3*	**1020,1**	*0,06*	**794,7**	*0,07*	**1017,1**	*0,06*	**0,22**	*1,6*	**100,2**	*1,2*	**16,9**	*1,9*
		90	**280,0**	*0,3*	**120,0**	*0,5*	**253,6**	*0,3*	**1019,9**	*0,06*	**794,8**	*0,07*	**1013,3**	*0,06*	**0,18**	*2,0*	**100,6**	*1,2*	**16,9**	*1,9*
		50	**200,0**	*0,3*	**200,0**	*0,3*	**100,9**	*0,6*	**1019,9**	*0,06*	**794,8**	*0,07*	**1017,3**	*0,06*	**0,26**	*1,4*	**101,4**	*1,2*	**16,8**	*1,9*
400	**50**	**70**	**200,0**	*0,3*	**200,0**	*0,3*	**140,0**	*0,5*	**1020,2**	*0,06*	**794,8**	*0,07*	**1004,8**	*0,06*	**0,19**	*1,9*	**103,4**	*1,2*	**16,8**	*1,9*
		90	**200,0**	*0,3*	**200,0**	*0,3*	**180,1**	*0,4*	**1020,1**	*0,06*	**794,8**	*0,07*	**983,6**	*0,07*	**0,20**	*1,8*	**101,9**	*1,2*	**16,8**	*1,9*
		50	**120,0**	*0,5*	**280,0**	*0,3*	**60,3**	*1,0*	**1020,7**	*0,06*	**795,3**	*0,07*	**1020,3**	*0,06*	**0,19**	*1,9*	**99,0**	*1,2*	**16,7**	*1,9*
	30	**70**	**120,0**	*0,5*	**280,0**	*0,3*	**83,8**	*0,7*	**1020,7**	*0,06*	**795,2**	*0,07*	**1018,4**	*0,06*	**0,22**	*1,7*	**98,1**	*1,2*	**16,7**	*1,9*
		90	**120,0**	*0,5*	**280,0**	*0,3*	**109,1**	*0,6*	**1020,5**	*0,06*	**795,1**	*0,07*	**1006,9**	*0,06*	**0,24**	*1,5*	**98,2**	*1,2*	**16,7**	*1,9*
		50	**350,0**	*0,2*	**150,0**	*0,4*	**176,2**	*0,4*	**1018,7**	*0,06*	**794,2**	*0,07*	**1016,4**	*0,06*	**0,21**	*1,8*	**100,6**	*1,2*	**17,2**	*1,9*
	70	**70**	**350,0**	*0,2*	**150,0**	*0,4*	**246,1**	*0,3*	**1019,5**	*0,06*	**794,2**	*0,07*	**1014,2**	*0,06*	**0,19**	*1,9*	**99,6**	*1,2*	**17,3**	*1,8*
		90	**350,0**	*0,2*	**150,0**	*0,4*	**318,0**	*0,2*	**1019,4**	*0,06*	**794,2**	*0,07*	**1005,9**	*0,06*	**0,21**	*1,7*	**99,5**	*1,2*	**17,3**	*1,8*
		50	**250,0**	*0,3*	**250,0**	*0,3*	**126,3**	*0,5*	**1018,8**	*0,06*	**794,3**	*0,07*	**1004,9**	*0,06*	**0,27**	*1,3*	**100,2**	*1,2*	**17,1**	*1,9*
500	**50**	**70**	**250,0**	*0,3*	**250,0**	*0,3*	**176,3**	*0,4*	**1019,3**	*0,06*	**794,3**	*0,07*	**978,7**	*0,07*	**0,19**	*1,9*	**101,1**	*1,2*	**17,1**	*1,9*
		90	**250,0**	*0,3*	**250,0**	*0,3*	**226,0**	*0,3*	**1019,8**	*0,06*	**794,4**	*0,07*	**963,6**	*0,06*	**0,18**	*2,0*	**101,3**	*1,2*	**17,2**	*1,9*
		50	**150,0**	*0,4*	**350,0**	*0,2*	**75,4**	*0,8*	**1020,6**	*0,06*	**794,9**	*0,07*	**1019,7**	*0,06*	**0,30**	*1,2*	**102,1**	*1,2*	**17,1**	*1,9*
	30	**70**	**150,0**	*0,4*	**350,0**	*0,2*	**104,6**	*0,6*	**1020,4**	*0,06*	**794,9**	*0,07*	**1015,5**	*0,06*	**0,25**	*1,5*	**103,2**	*1,2*	**17,1**	*1,9*
		90	**150,0**	*0,4*	**350,0**	*0,2*	**134,9**	*0,5*	**1020,1**	*0,06*	**794,8**	*0,07*	**1002,0**	*0,06*	**0,20**	*1,8*	**102,4**	*1,2*	**17,1**	*1,9*

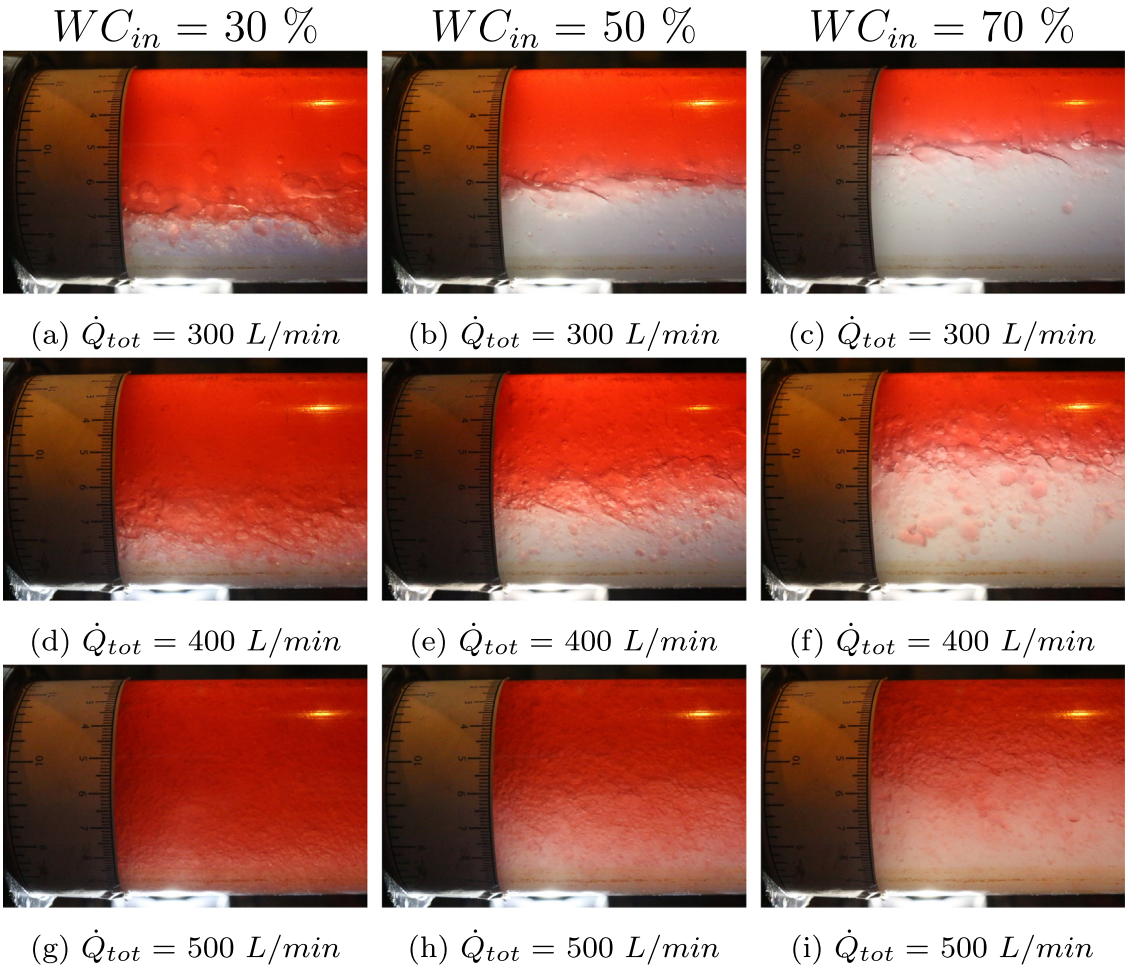

Fig. A.21. Inlet flow regime for open choke valve with no surfactant test points.

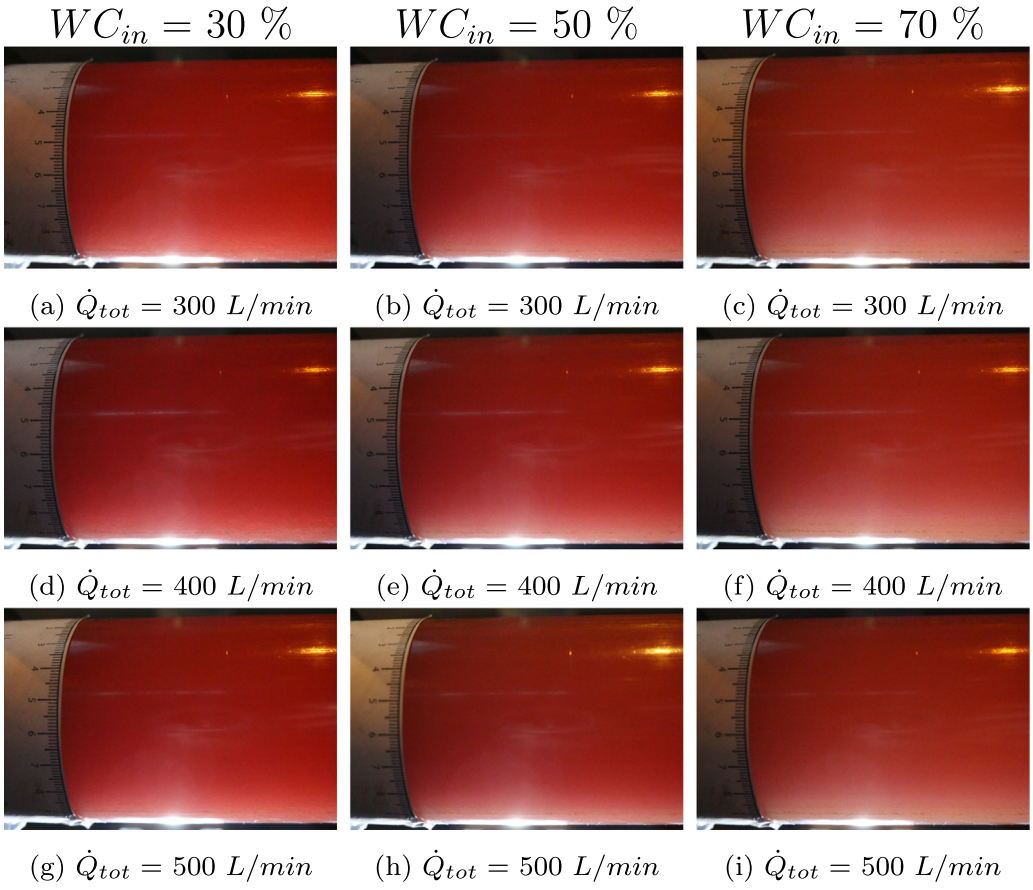

Fig. A.22. Inlet flow regime for $dPT.1 = 100$ mbar with 15 ppm Span®85 test points.

Table A.12
Bottom location d_{v50} [μm] data for **no surfactant** and *surfactant* test points.

WC_{in} [%]	$dPT.1$ [mbar]	Total flow rate [L/min]					
		300		400		500	
	–	**199.1**	*42.1*	**235.6**	*145.8*	**148.6**	*247.2*
30	50	**290.3**	*300.8*	**290.5**	*271.8*	**262.6**	*256.3*
	100	**251.5**	*259.3*	**250.7**	*258.5*	**234.9**	*244.0*
	–	**64.4**	*59.2*	**60.5**	*72.5*	**71.4**	*123.2*
50	50	**335.1**	*297.2*	**295.1**	*283.1*	**278.2**	*261.6*
	100	**282.0**	*285.6*	**268.9**	*255.4*	**266.3**	*233.2*
	–	**43.3**	*52.7*	**61.5**	*81.4*	**69.4**	*72.5*
70	50	**268.6**	*257.5*	**260.7**	*250.1*	**254.4**	*231.9*
	100	**247.7**	*244.3*	**237.0**	*204.7*	**194.4**	*185.8*

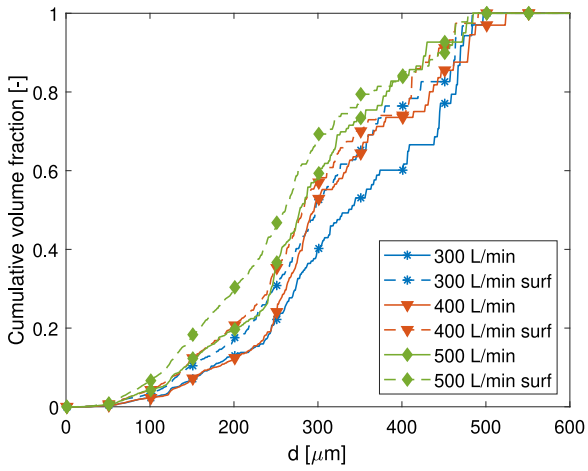

Fig. A.23. Cumulative volume fraction for WC_{in} = 50 %, $dPT.1$ = 50 mbar.

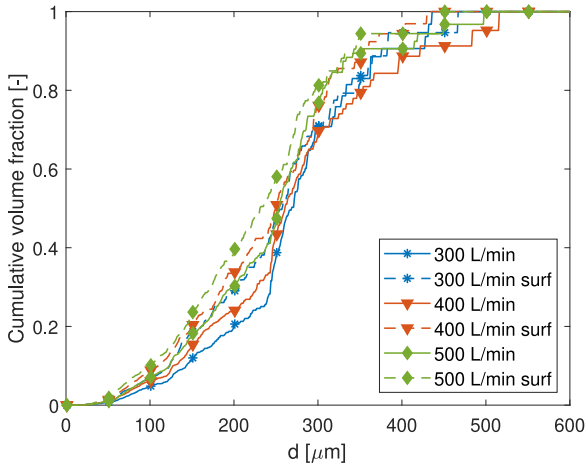

Fig. A.24. Cumulative volume fraction for WC_{in} = 70 %, $dPT.1$ = 50 mbar.

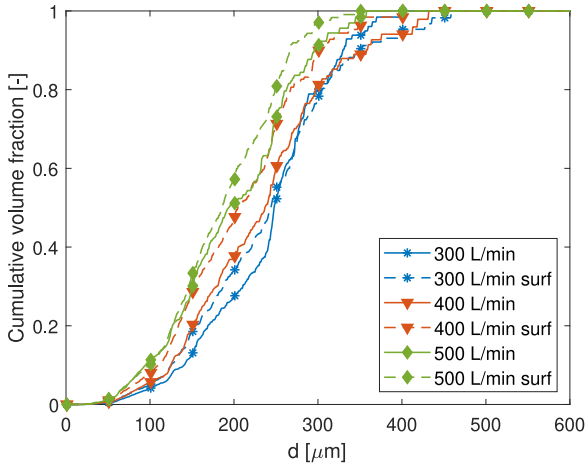

Fig. A.25. Cumulative volume fraction for WC_{in} = 70 %, $dPT.1$ = 100 mbar.

References

Andresen, P.A.K., Arntzen, R., Sjøblom, J., 2000. Stability of model emulsions and determination of droplet size distributions in a gravity separator with different inlet characteristics. Colloids Surf. A 170 (1), 33–44.

Angeli, P., Hewitt, G.F., 2000. Drop size distributions in horizontal oil-water dispersed flows. Chem. Eng. Sci. 55 (16), 3133–3143.

Backi, C.J., Grimes, B.A., Skogestad, S., 2018. A control-and estimation-oriented gravity separator model for oil and gas applications based upon first-principles. Ind. Eng. Chem. Res. 57 (21), 7201–7217.

Bliatsiou, C., Malik, A., Böhm, L., Kraume, M., 2018. Influence of impeller geometry on hydromechanical stress in stirred liquid/liquid dispersions. Ind. Eng. Chem. Res..

Bringedal, B., Ingebretsen, T., Haugen, K., et al., 1999. Subsea separation and reinjection of produced water. In: Offshore Technology Conference.

Dudek, M., Bertheussen, A., Dumaire, T., Øye, G., 2018. Microfluidic tools for studying coalescence of crude oil droplets in produced water. Chem. Eng. Sci. 191, 448–458.

Dudek, M., Kancir, E., Øye, G., 2017. Influence of the crude oil and water compositions on the quality of synthetic produced water. Energy Fuels 31 (4), 3708–3716.

Fossen, M., Arntzen, R., Hemmingsen, P.V., Sjöblom, J., Jakobsson, J., 2006. A laboratory-scale vertical gravity separator for emulsion characterization. J. Dispers. Sci. Technol. 27 (4), 453–461.

Fossen, M., Schümann, H., 2017. Experimental study of the relative effect of pressure drop and flow rate on the droplet size downstream of a pipe restriction. J. Dispers. Sci. Technol. 38 (6), 826–831.

NOROG, 2017. 2017 Environmental Report - Environmental Work By the Oil and Gas Industry, Facts and Development Trends. Technical Report. NOROG.

Panckow, R.P., Reinecke, L., Cuellar, M.C., Maaß, S., 2017. Photo-optical in-situ measurement of drop size distributions: applications in research and industry. Oil Gas Sci. Technol. 72 (3), 14.

Riegler, P., Chrusciel, T., Mayer, A., Doll, K., Weuster-Botz, D., 2019. Reversible retrofitting of a stirred-tank bioreactor for gas-lift operation to perform synthesis gas fermentation studies. Biochem. Eng. J. 141, 89–101.

Schümann, H., Khatibi, M., Tutkun, M., Pettersen, B.H., Yang, Z., Nydal, O.J., 2015. Droplet size measurements in oil–water dispersions: A comparison study using FBRM and PVM. J. Dispers. Sci. Technol. 36 (10), 1432–1443.

Skjefstad, H.S., Stanko, M., 2017. Subsea water separation: a state of the art review, future technologies and the development of a compact separator test facility. In: 18th International Conference on Multiphase Production Technology. BHR Group.

Skjefstad, H.S., Stanko, M., 2018. An experimental study of a novel parallel pipe separator design for subsea oil-water bulk separation. In: SPE Asia Pacific Oil and Gas Conference and Exhibition. Society of Petroleum Engineers.

Skjefstad, H.S., Stanko, M., 2019. Experimental performance evaluation and design optimization of a horizontal multi-pipe separator for subsea oil-water bulk separation. J. Petrol. Sci. Eng..

Tichelkamp, T., Teigen, E., Nourani, M., Øye, G., 2015. Systematic study of the effect of electrolyte composition on interfacial tensions between surfactant solutions and crude oils. Chem. Eng. Sci. 132, 244–249.

Trallero, J., Sarica, C., Brill, J., et al., 1997. A study of oil-water flow patterns in horizontal pipes. SPE Prod. Facil. 12 (03), 165–172.

Wong, S., Lim, J., Dol, S., 2015. Crude oil emulsion: A review on formation, classification and stability of water-in-oil emulsions. J. Petrol. Sci. Eng. 135, 498–504.

Zolfaghari, R., Fakhru'l-Razi, A., Abdullah, L.C., Elnashaie, S.S., Pendashteh, A., 2016. Demulsification techniques of water-in-oil and oil-in-water emulsions in petroleum industry. Sep. Purif. Technol. 170, 377–407.